Geophys. J. Int. (1994) **119,** 453–478

Complex structure along a Mesozoic sea-floor spreading ridge: BIRPS deep seismic reflection, Cape Verde abyssal plain

J. H. McBride,[1] R. S. White,[2] T. J. Henstock[2,*] and R. W. Hobbs[1]

[1] *British Institutions Reflection Profiling Syndicate, Bullard Laboratories, Department of Earth Sciences, University of Cambridge, Madingley Road, Cambridge* CB3 0EZ, *UK*

[2] *Bullard Laboratories, Department of Earth Sciences, University of Cambridge, Madingley Road, Cambridge* CB3 0EZ, *UK*

Accepted 1994 March 24. Received 1994 March 1; in original form 1993 September 22

SUMMARY

As part of an intensive study of a small area of oceanic lithosphere, the British Institutions Reflection Profiling Syndicate (BIRPS) acquired closely spaced deep-seismic-reflection profiles over the Early Cretaceous crust of the Cape Verde abyssal plain off West Africa. The survey consisted of profiles spaced at 4 km arranged into strike lines parallel to the old sea-floor spreading axis ('isochron' profiles) and orthogonal dip lines oriented in the original direction of spreading ('flow' profiles). A large-capacity, well-tuned airgun source and very quiet shooting conditions ensured a high signal-to-noise ratio for deep reflection. Devising a strategy for mitigating contamination from 'wrap-around' multiples arriving from previous shots enabled us to use the minimum possible shot-point interval (50 m) allowed for collecting long (18 s) records. Data processing was oriented towards a medium with low root-mean-square velocity, steeply dipping structure, and pervasive low apparent velocity noise from diffraction at the top of the igneous crust. The contrast between the isochron and flow profiles is striking. Isochron profiles are typically highly reflective throughout the igneous crust, consisting of bright, bidirectionally dipping reflection sets that extend in places from the top of the igneous basement down to the interpreted Moho reflection. These reflections do not offset intracrustal or top-basement structure and thus are not interpreted as faults: an igneous intrusive origin seems more likely. Flow profiles are more sparsely reflective but show individual steeply dipping reflections best developed in the upper igneous crust, continuing down in places to the Moho. Dipping reflections on the flow profiles are interpreted as major normal faults since they are clearly associated with offsets of the top of the basement as well as truncation of horizontal reflections within the igneous crust. The dominant dip of these reflections is to the west towards the spreading ridge axis. Reflections from the vicinity of the Moho, while well developed in some places, are not particularly prominent across the survey area. Moho reflections appear to show a different structural relation to crustal features on the isochron and flow profiles: on isochron profiles, dipping reflections occasionally flatten out into, and may merge with, the Moho reflection; on flow profiles, as dipping crustal reflections approach the Moho reflection, they are usually abruptly cut off by it without extending deeper. This survey shows how oceanic crustal structure can vary rapidly over relatively small areas, provides convincing evidence that a structurally complex fabric dominates oceanic igneous crust, and gives a conclusive observation of faults that penetrate the entire oceanic crust.

Key words: deep seismic reflection, Early Cretaceous Mid-Atlantic ridge, normal faults.

* Now at: Department of Earth Sciences, Parks Road, University of Oxford, Oxford OX1 3PR, UK.

INTRODUCTION

The past decade has seen the increased application of deep-seismic-reflection profiling in the deep sea over oceanic lithosphere. Most of these programmes have relied on vessels deploying smaller sources and fewer receivers, compared to commercial operations, and have targeted anomalous features such as fracture zones, active mid-ocean ridges, and structures associated with subduction zones. The survey layouts have usually been limited to single long reconnaissance or widely spaced parallel lines, often oriented obliquely to structural trends. In September 1991, the British Institutions Reflection Profiling Syndicate (BIRPS) recorded 578 km of deep-reflection data over a small area of the Cape Verde abyssal plain using a combination of closely spaced strike- and dip-parallel lines. The survey was concentrated over an area of crust believed to have a relatively simple tectonic history, avoiding major fracture zones, and located approximately 2200 km east of the active Mid-Atlantic spreading ridge. The rationale of the programme was to characterize the detailed 3-D structure of oceanic crust and uppermost mantle unaffected by major tectonism or magmatism since the time of original construction at the spreading ridge. The purpose of this paper is to (1) outline the essential features of the BIRPS deep seismic experiment emphasizing those aspects governed by the nature of the target, (2) discuss briefly the role of data processing for imaging of complex structure in oceanic crust, and (3) summarize the more important results of the survey, especially the interpretation of dipping reflections within the igneous crust.

The survey was located over Early Cretaceous oceanic crust (Fig. 1a) west of the West African magnetic quiet zone boundary (Hayes & Rabinowitz 1975). The geophysical and tectonic setting of the area has been discussed by Sundvik & Larson (1988), Dañobeitia & Collette (1989), Williams *et al.* (1990), Dañobeitia & Rivero (1991), Verhoef *et al.* (1991), and Roest *et al.* (1992). Plate reconstructions along fracture zones (Klitgord & Schouten 1986) show the survey site to be conjugate to an area off the central East Coast of the USA along strike of a previous set of seismic programmes over the Blake Spur fracture zone region (NAT Study Group 1985; White *et al.* 1990; Morris *et al.* 1993). Information from nearby Deep Sea Drilling Project (DSDP) sites (Nos 139 & 140, Hayes *et al.* 1972) indicates flat-lying sediments between 1500 and 2000 m thick, recent to Maastrichtian in age (Fig. 1a). Calibration of sea-floor spreading magnetic anomalies suggests a full spreading rate of about 20 mm yr^{-1} for the Early Cretaceous (Kent & Gradstein 1985) which would be classified as a slow-spreading ridge system (White 1984). The seismic-reflection survey was preceded by a site-preparation survey in January 1991 that collected magnetic intensity, gravity, and bathymetric data (Henstock, White & McBride 1994). These data were used to locate the positions of magnetic anomalies and major fracture zones. From the magnetic survey, we accurately located the *M*-15 and *M*-16 sea-floor spreading magnetic anomalies corresponding to one side of the Early Cretaceous mid-oceanic spreading centre along which we laid out our orthogonal set of reflection lines (Fig. 1b). A major fracture zone, which can be traced from north of Bermuda to north of Cap Blanc on smaller-scale maps (Klitgord & Schouten 1986), was identified along the northern end of the survey area. A small-offset fracture zone, or possibly a minor non-transform discontinuity (e.g. Sempéré *et al.* 1993), was recognized from the magnetic data over a portion of the southern part of the survey between and including the western parts of Lines 8–10 (Fig. 1b). Water depth varies gradually from 4700 m in the eastern part of the area to 4900 m in the west.

Previous reflection surveys in the North Atlantic have consisted of single reconnaissance lines (NAT Study Group 1985; Peddy *et al.* 1990; Banda *et al.* 1992) or widely spaced parallel or subparallel lines (Rosendahl *et al.* 1990; Maschenkov & Pogrebitsky 1992; Morris *et al.* 1993). Although these surveys revealed combinations of dipping and horizontal structures, these remained enigmatic since they could not be traced onto parallel or crossing lines. Interpretation of most of these surveys was also hampered by a line orientation that was oblique to the known sea-floor spreading direction. Such factors have contributed to widely varying interpretations of structures that are too complex to be understood using a reconnaissance approach. One of the aims of the current programme was to overcome these difficulties by using a more closely spaced layout of strike and dip lines, and to orient these lines precisely along and perpendicular to the original sea-floor spreading direction.

DESIGN OF EXPERIMENT

Source and receiver

As with previous BIRPS experiments, success depended upon a seismic source suitable for imaging lower crustal and upper mantle structure. Our strategy began with designing a tuned airgun-source array rich in low frequencies corresponding to the expected returning signal from the lower crust and uppermost mantle while retaining enough high frequency to image detail in the sedimentary section such as small fault offsets and unconformities (e.g. Hobbs & Snyder 1992). In most deep crustal environments, bandwidth is limited by attenuation to frequencies less than about 35 Hz (Scheirer & Hobbs 1990). Several combinations of airgun-array capacity, element configuration, and source depth were modelled using synthetic-source signatures and amplitude spectra. The final selected source was a 36-element array towed at 7.5 m depth with a total volume of ~117 litres (7118 in^3) at a nominal pressure of ~13.8 MPa (2000 psi) using GECO-PRAKLA's M/V *Bin Hai* 511. The low-frequency component is apparent in the enhanced bubble pulse in the gun array signature (Fig. 2). The amplitude spectrum has a broad peak over the range 8 to 20 Hz. For higher frequencies, some notching of the spectrum was unavoidable and we chose a source that minimized this effect. Peak-to-peak amplitude was 116.6 bar m (0–128 Hz) or, for the recording filters (5.3–64 Hz), 70.9 bar m (Fig. 2) which is high compared to standard industry exploration surveys (Dragoset 1990).

Because the amplitude of signal from the lower crust is orders of magnitude less than that from sediments, we required a receiver cable with low noise specifications (Table 1) operating in an environment where ambient pressure on the hydrophone groups does not exceed a few μbars. Higher noise levels could overwhelm Moho reflections for which peak-to-peak amplitude at near-normal incidence is only a few μbars (Hobbs & Snyder 1992). Because shooting conditions during the survey were ideal with uniformly calm weather and no ship traffic, we were able to keep average noise levels to less than 2 μbars (Fig.

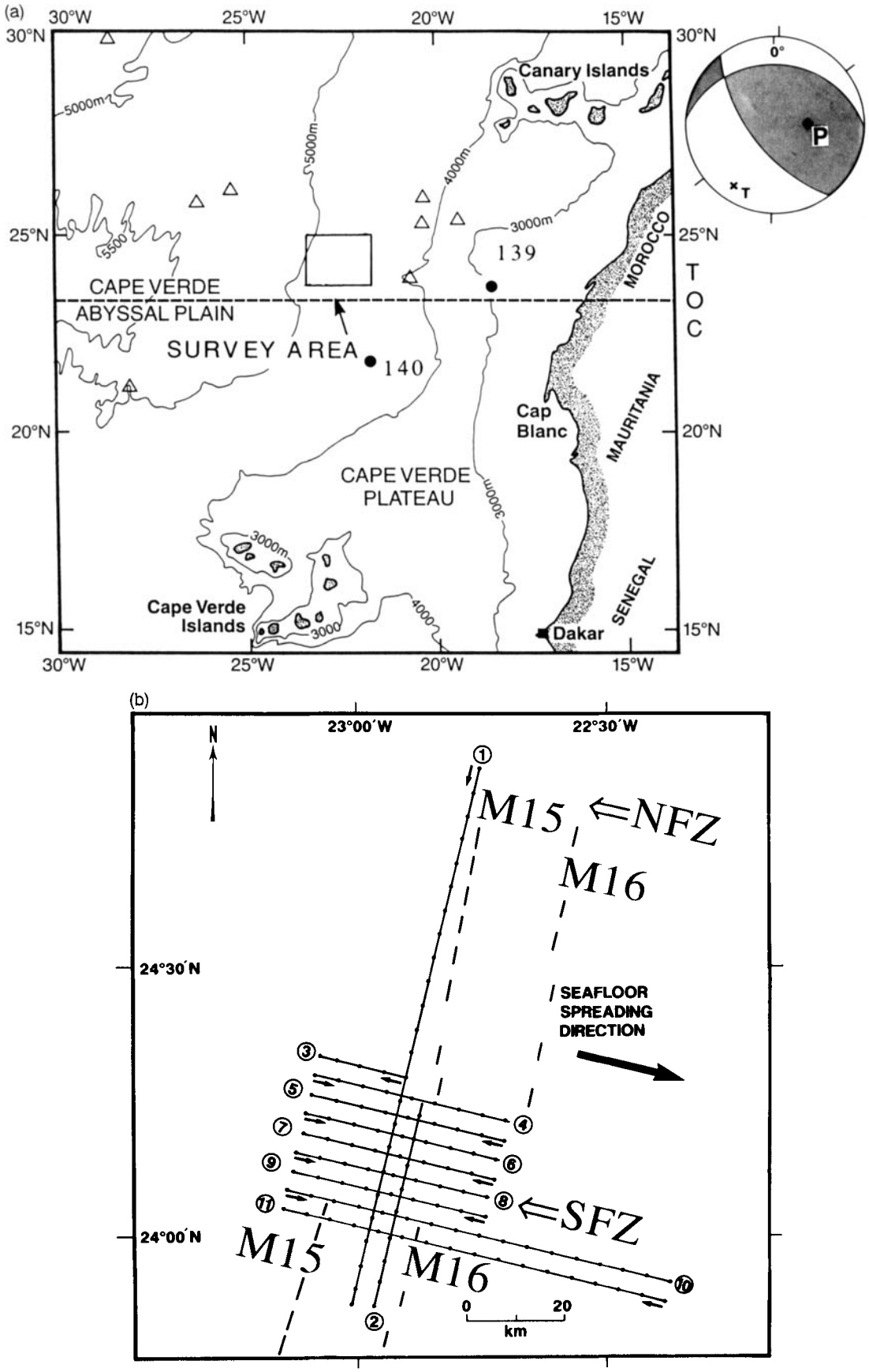

Figure 1. (a) General location map for study area. Black circles: DSDP sites. Triangles: major seamounts. TOC: Tropic of Cancer. Stereogram centroid-moment-tensor focal mechanism solution of magnitude 5.2 earthquake near the Canary Islands (Date: 1989 5 9; Location: 28°02′N, 16°10′W) from the International Seismicity Catalogue. (b) Survey line lay-out with sea-floor spreading magnetic lineations interpreted from a magnetic survey, 1991 January. Dots along lines represent shot-point locations marked every 100 points, beginning with 1 at the start of each line (arrows). NFZ: northern fracture zone. SFZ: southern fracture zone.

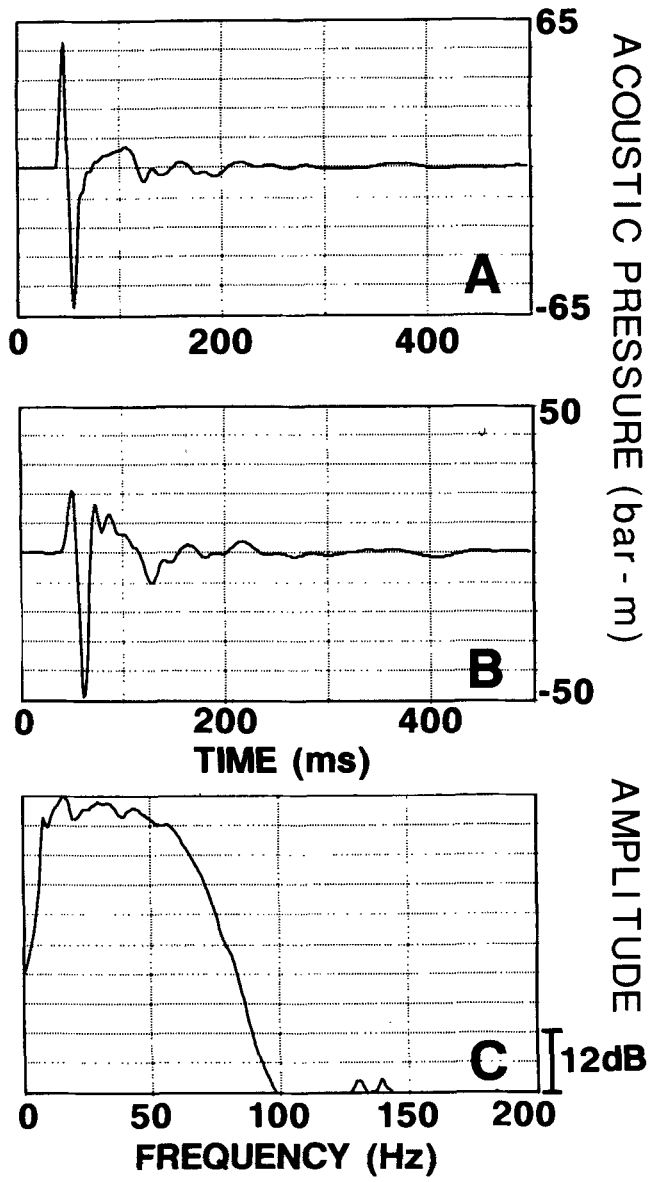

Figure 2. Results of modelling the airgun-source array. (a) Array signature, 0–128 Hz. (b) Signature 5.3 Hz/18 dB per octave −64 Hz/72 dB per octave (shipboard recording filters). (c) Amplitude spectrum of (b). dB referred to μPa/Hz at 1 m.

3). The 4500 m long receiver cable contributed to multiple attenuation and increased signal-to-noise ratio (s/n) during common mid-point (CMP) stacking. The deep tow of the cable enhanced low frequencies while avoiding noise from near-surface turbulence (e.g. from the large source array itself). Because of the possibility of irregularities in the top of the igneous basement that could produce out-of-the-plane reflection or scattering, we deployed a wide, 60 m source array to control the directivity of the far-field signal (e.g. Parkes & Hatton 1986).

Survey plan

As mentioned above, previous programmes have generally been ineffective in tracing observations between lines. In an attempt to overcome this, we spaced lines close enough to maximize the chances of correlating structure but enabling as much regional coverage as possible. The 4 km line spacing approximately matches the expected Fresnel Zone diameter for lower crustal frequencies (Raynaud 1988). Two strike (or 'isochron') profiles approximately parallel to sea-floor spreading magnetic anomalies (and thus parallel to the old ridge axis) and nine orthogonal dip (or 'flow') profiles parallel to the original direction of sea-floor spreading were surveyed (Fig. 1b). The record length was 18 s (two-way traveltime), and the shot-point interval was 50 m.

Table 1. Acquisition parameters for BIRPS seismic-reflection survey.

ACQUISITION PARAMETERS	
Recording Instrument	DFS V/GDR 1000
Record Length	18 s
Sample Rate	4 ms
High Cut Filter/Slope	64 Hz/72 dB
Low Cut Filter/Slope	5.3 Hz/18 dB
Shotpoint Interval	50 m
Monitor Record	Every 20 shots
Primary Navigation	GPS
Antenna-Source Cent.	119 m
Antenna-Near Trace	250 m
Total Airgun Volume	7118 in^3 ~117 l
Nominal Pressure	2000 p.s.i. ~13.8 MPa
Airgun Array Depth	7.5 m
Number of Guns	36
Array Width	60 m
Receiver Cable Type	HSSQ
Hydrophones/Group	40
Number of Groups	180
Group Length	25 m
Cable Depth	15 m
Depth Transducers	20 Along Cable
Length Active Cable	4501 m
Total Length of Line	578 km
Date of Survey	September 1991
Contractor	GECO-PRAKLA
Vessel	M/V *Bin Hai* 511
Client	BIRPS

The 'wrap-around' multiple problem

Owing to water depths of almost 5000 m, multiple reflections can bounce within the water column for long periods without the loss of amplitude that would otherwise accrue in shallow water where the multiple series dies out quickly. In deep water, the time delay between successive shots is much less than the time required for the multiple series to lose significant amplitude relative to the primaries, so that contamination of the shot records by multiples from

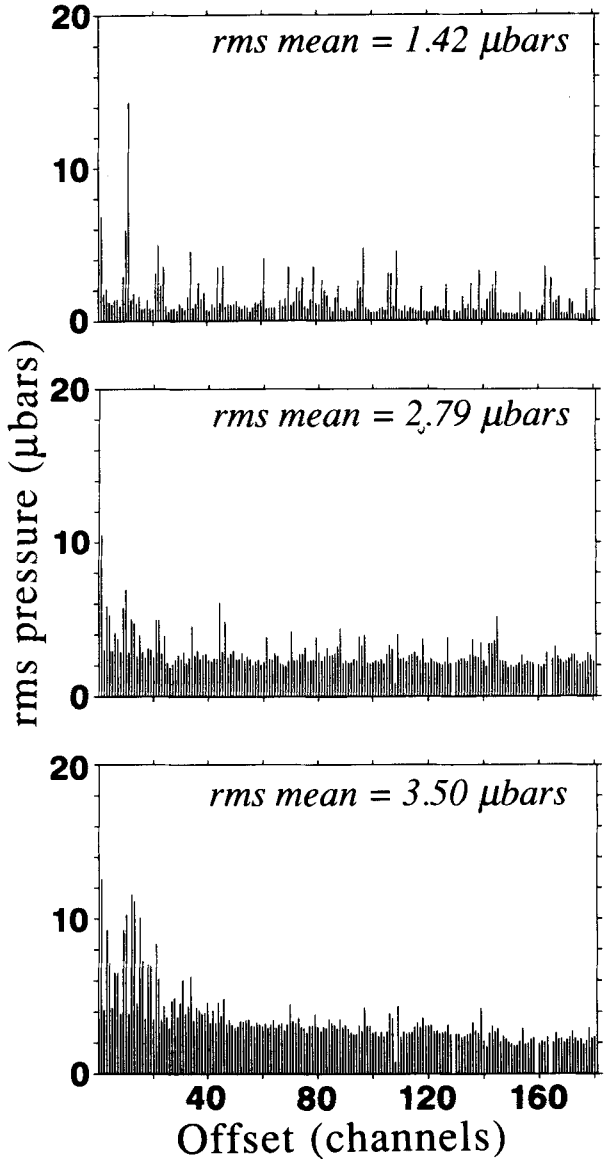

Figure 3. Noise tests on 180-channel receiver cable with rms mean pressure for Line 11 over 4–5 s time interval in the water column. Top: before firing airguns at start of line. This approximates 'ambient' level of noise. Middle: during noise recording in middle of survey while missing one shot (e.g. as in Fig. 4). Bottom: during active shooting and recording.

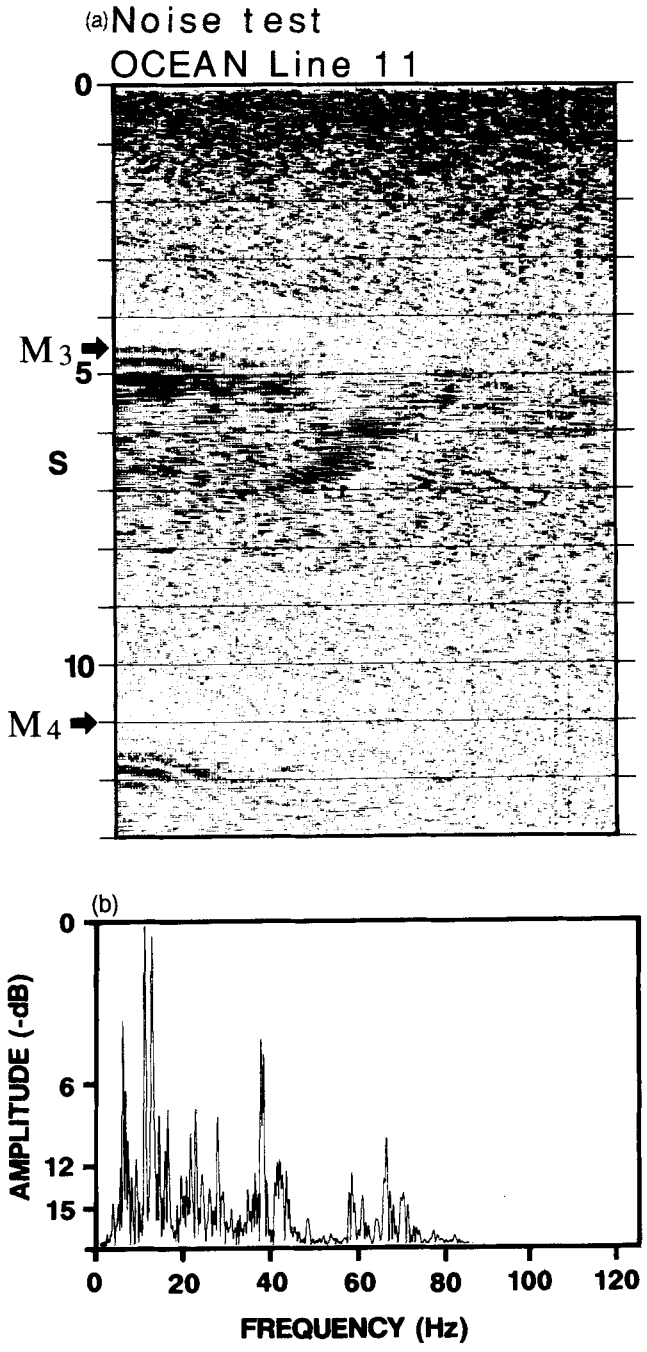

Figure 4. (a) Noise-test record (shot point 589, Line 11) made by recording without a shot, showing the high-amplitude and coherent wrap-around multiple reflections. The third and fourth multiple series generated by the sediments (M_3 and M_4) have arrived from the shot fired 21.66 s earlier. For display purposes, the record has been bandpass filtered 30–60 Hz, a linear gain has been applied, and a variable area no wiggle trace mode used. Record is displayed for all 180 channels. (b) Frequency spectrum for M_3 multiple series. Note difficulty of isolating multiples in frequency.

previous shots is likely ('wrap-around' multiples; McBride *et al.* 1994a). Noise records (Fig. 4a), produced by recording in sequence without a shot, clearly show the resilience of the wrap-around multiples, which contain a broad band of frequencies making them difficult to remove by filtering (Fig. 4b). Because these multiples travel for such long times (e.g. M_4, Fig. 4a), they cannot be easily discriminated from primary reflections on the basis of normal move-out (NMO) and so are not susceptible to attenuation by stacking (Levin 1971). We took a two-step approach to alleviating the wrap-around multiple problem. While primarily controlling the shot interval on the basis of GPS navigation, we first imposed a nominally constant shot-time delay of 21 s in order to monitor the multiples and to place them where they would cause the least contamination of primary reflections (Fig. 5). The second step introduced a pseudo-random time delay (1–255 ms) trigger device inserted between the ship's

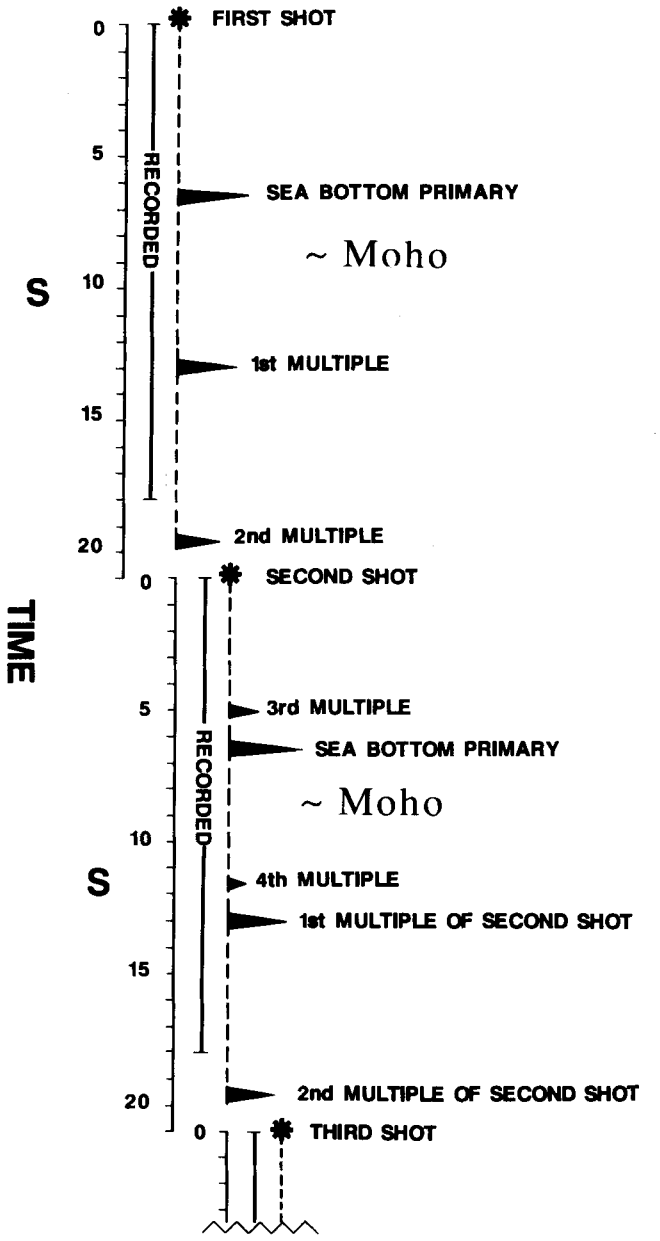

Figure 5. Diagram showing arrival times of sea-bottom multiples and primaries through two consecutive shot recordings using the fixed shot time delay of 21 s chosen for the BIRPS reflection survey where water depths are about 4900 m.

navigation computer output and the profiling system (McBride *et al.* 1994b). Superimposing this delay on the 21 s shot time decreases the coherency of the multiples by destructive interference as they are CMP-sorted and stacked (Fig. 6). In a few instances, multiple cancellation is incomplete over the 11–13 s interval (Fig. 7a); however, the randomization has reduced the level of amplitude, periodicity, and coherency to well below that which would otherwise have developed if the multiples had added constructively (Fig. 7b).

DATA PROCESSING

The unusual nature of the target required special emphasis to be put on some of the processing steps (Table 2). The combined factors of deep water and a low-velocity sediment cover served to lower the root-mean-square (rms) velocity in the igneous crust; NMO sensitivity persisted to 9–10 s. Velocity analysis was aimed principally at enhancement of complex dipping structure in the igneous crust, attenuation of pegleg multiples from the sediments, and definition of diffractions at the sediment–basement interface (e.g. McBride *et al.* 1993). Because of the extended NMO sensitivity, it was possible in places to identify candidate reflections from the Moho discontinuity with rms velocities of 3300–3500 m s^{-1} (Fig. 8a) (*cf.* Tsai 1985). However, accurate derivation of interval velocities for the igneous basement was often hindered by complex, steeply dipping reflector structure and by diffractions. Time-to-depth conversion and measurement of angles on the migrated sections are made using the smoothed interval velocities (Fig. 8b). After velocity analysis, we experimented with range-limited stacking in order to produce a more 'accurate' CMP stack for studying faults (minimizing NMO stretch and stacking of non-hyperbolic events) and for assessing out-of-plane effects. The near 30-channel stacks (Fig. 9) produce a less complex picture of high-amplitude dipping reflections in the upper igneous crust but with an overall loss of s/n deeper. For deep targets, stacking shorter offsets produces an approximately '1-D' view with increased horizontal resolution but at the possible expense of vertical resolution (Levander *et al.* 1994).

Because of the characteristic surface roughness of oceanic igneous crust, the lower part of the CMP stack is dominated by diffractions and associated low apparent velocity noise (Fig. 10). Although migration collapses some of the diffracted energy, much of the low apparent velocity noise remains, severely obscuring primary events (Fig. 10a, c) (Larner *et al.* 1983; Newman 1984). A post-stack frequency-wavenumber (f–k) filter and series of bandpass filters (Table 2) applied prior to migration removed most of this noise while leaving a sufficient portion of the diffraction energy for the migration operator (Fig. 10b). A relatively simple deconvolution was applied to reduce contamination from interbed multiples and to help balance the frequency spectrum (Fig. 11). Owing to the high noise content in reflections from the igneous crust, only a post-stack predictive deconvolution was applied with a relatively wide gap (or 'lag'). A particular problem was the presence of a diffractive (or 'scattering') layer at about 300 ms below the seabed which tended to produce an inaccurate operator design resulting in a somewhat erratic and incoherent reflection character for the sediments (Fig. 11). The origin of the scattering layer is unknown; information from DSDP Site 139 (Hayes *et al.* 1972) shows only a monotonous series of Pliocene calcareous nanofossil ooze over this interval. The problem was partially alleviated by using a shortened operator length and applying the deconvolution over a 50-trace averaged window (Fig. 11). Finally, constant-velocity f–k migrations (Stolt 1978) were used to derive readily a practical velocity for 2-D 15° finite-difference migration (Claerbout 1985) based on smoothed velocities from stacking velocity analysis. Both

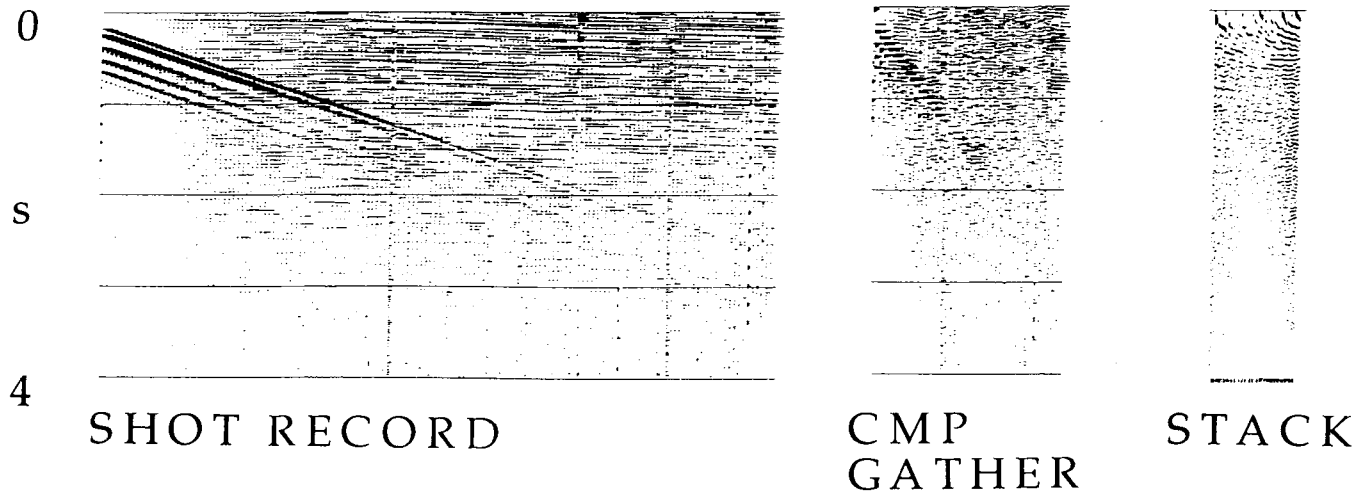

Figure 6. Left: shot record (180 channels, 4500 m) with strong wrap-around multiples produced in the water column by a previous shot fired ~21 s ago (see Fig. 5). Middle: CMP gather (45 fold, 12.5 m bin size) centred over the shot shown in (a). Note break-up of lateral coherency of wrap-around multiples due to randomization of the shot-time interval delay. Right: stacked section (using CMP traces 20–45) centred over CMP gather in (b) with multiples largely broken up.

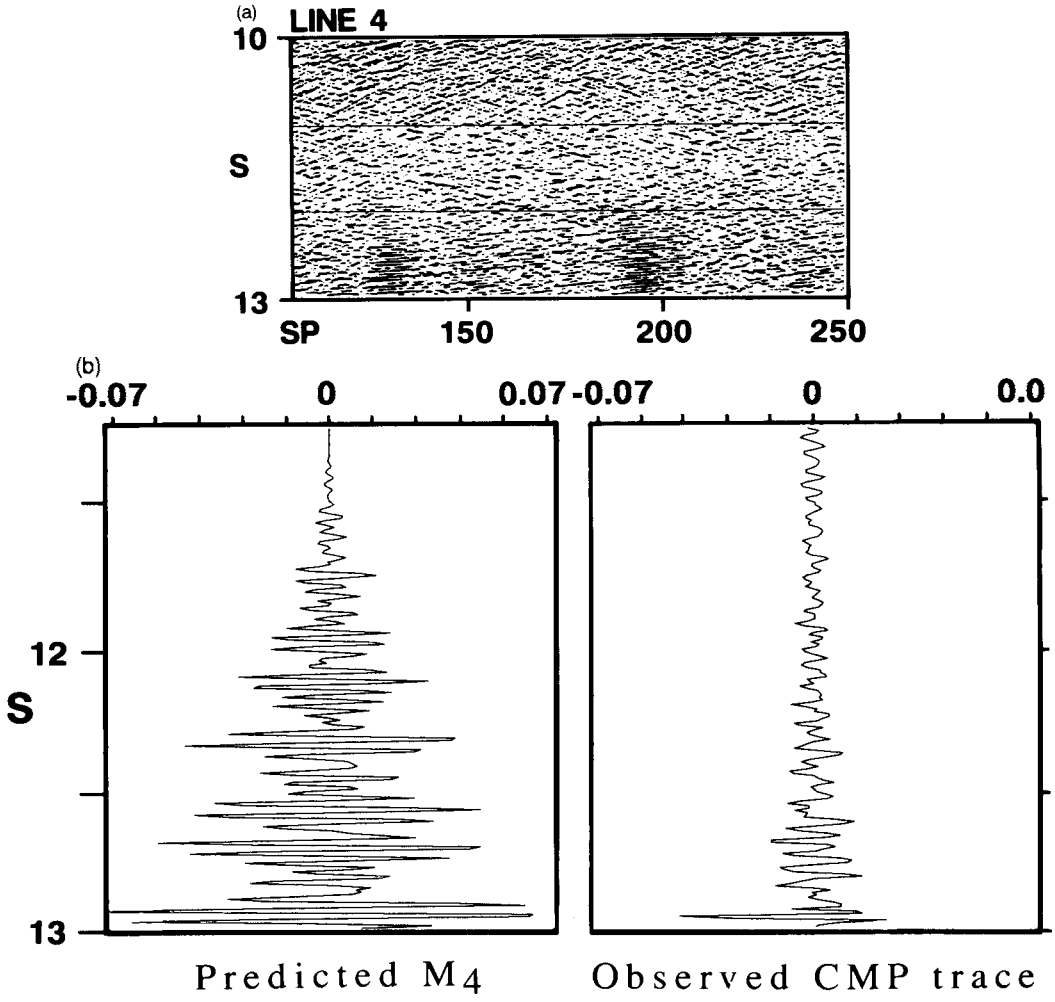

Figure 7. (a) Portion of unmigrated Line 4 stack displayed with high gain showing coherent wrap-around multiples between 11.5 and 13 s. Out of the entire survey this area experienced the worst effects of the wrap-around multiple problem. This and other CMP stacked time sections are displayed with no vertical exaggeration at 6 km s^{-1}. The shot-point interval is 50 m. (b) Comparison of observed CMP trace from near shot-point 190 from (a) and the predicted fourth wrap-around multiple reflection (M_4). M_4 is computed using an autoconvolution generated from the deconvolved sedimentary section of the CMP trace (see McBride *et al.* 1994b). The predicted M_4 would have resulted if multiples had not been broken up by a randomization of the shot time interval (i.e. if they had added constructively in the CMP domain). Horizontal scale is a model reflection coefficient.

Table 2. Data processing parameters for BIRPS seismic-reflection survey.

PROCESSING HISTORY

1	Re-sample	From 4 ms to 8 ms; processed 13-s record.
2	Amplitude compensation	Gain (dB) = 2.0 × traveltime + 45.
3	Common mid-point sort	180 channels, 45 fold.
4	Normal move-out correction	Stacking velocities defined every 10.5 km, ave.
5	Inner trace mute	(92 m, 6.0 s) (4725 m, 6.0 s) taper = 120 ms.
6	Common mid-point stack	Remove step 2. Spherical divergence correction.
7	Datum correction	Static correction for source & streamer: + 15 ms.
8	Frequency-wavenumber filter	Pie-slice filter: ± 3.5 ms/trace — ± 60 ms/trace.
9	Predictive deconvolution	0-8.4 s: Operator = 144 ms; Gap = 32 ms. 8.0-13.0 s: Operator = 216 ms; gap = 48 ms. Design windows: 6.5-8.4 s, 8.5-11 s. White noise = 1 %, overlap zone = 400 ms.
10	Frequency filters	6-7 s: 12 Hz out; 7-8 s: 12-40 Hz; 8-10 s: 5.3-24 Hz; 10-13 s: 5.3-17 Hz.
11	Amplitude compensations	Exponential gain; time-varying gain (redesigned for each line); automatic gain control 1500 ms.
12	15° Finite-difference migration	Applied using smoothed 2-D velocity field.
13	Display	Variable area, no wiggle, large negative trace gain bias. Exceptions where noted.

migrated and unmigrated versions of the stacks were used for interpretation. Some previous programmes have applied 'coherency filters' to the stacked data in order to enhance reflections in the igneous crust. Because such filters can in practice produce artefacts caused by lateral smearing, we have avoided them.

RESULTS AND INTERPRETATION

General features

Assuming the features under investigation originated at the Mid-Atlantic ridge, the arrangement of the seismic profiles into long strike (isochron) and short dip (flow) profiles allows us to compare structures that formed synchronously with those that formed sequentially. The strike profiles follow a line of more or less constant geologic time, so that they represent structure produced at the same time along the old spreading ridge. In the same way, the orthogonal dip lines indicate structures produced over a range of time. Using a sea-floor half-spreading rate of $10\,mm\,yr^{-1}$, the 40 km long dip profiles chart 4 million years of ocean crust formation.

The profiles (Fig. 12) are generally very reflective from the seabed, at about 6.5 s down to 9.8–10.0 s; the reflectivity of the strike lines extends further, as much as 12 s. The well-layered series of mainly horizontal reflections between the seabed and about 8 s is readily interpreted as sedimentary and, on the basis of interval velocities extracted from velocity analysis (Fig. 8a), has a thickness over most of the profiles ranging from about 800 to 1500 m with variation becoming more extreme to the south. DSDP seismic reflection records from Site 139 show a strong reflection at about 0.6 s below the seabed which correlated in the drill hole with a weakly expressed downward change from calcareous nanofossil ooze to increased amounts of quartz sandstone near the Middle/Lower Miocene boundary (Hayes *et al.* 1972). The sediment series on the profiles consists of two broad layers distinguished by interval velocity and separated by a prominent high-amplitude and continuous reflection (Fig. 8b) which may be analogous to the DSDP '0.6 s' reflection. Whitmarsh, Miles & Pinheiro (1990) suggested that similar high-amplitude reflections occurring in the middle of the sedimentary section in deep-water oceanic environments mark a strong increase in compaction. The diffractive surface underlying the sediment series marks a jump in rms velocity typically of about 1620 to 1700–1800 $m\,s^{-1}$ (corresponding to an interval velocity change from 2420 $m\,s^{-1}$ to ~5900 $m\,s^{-1}$) and is characteristic of the boundary between sediments and oceanic igneous basement. This surface was very sensitive to migration velocity with variations of ±50 $m\,s^{-1}$ being significant.

Figure 8. (a) Example of velocity semblance analysis. The starting velocity function estimate is given by the dashed line (0 per cent). Solid lines are velocity functions at ±10 per cent increments. The strong semblance peak at 9.75 s at a stacking velocity of 3300–3400 $m\,s^{-1}$ matches interpreted Moho reflections on the stacked CMP section. (b) Example of composite velocity function used for computing depths and angles on the stacked sections, and for guiding choice of migration-velocity functions. Sediment velocities derived from stacking-velocity analysis (converted to interval velocities using Dix equation); igneous crust portion derived from forward modelling of refracted arrivals using long-offset recordings from a later seismic experiment (Henstock, White & McBride 1994).

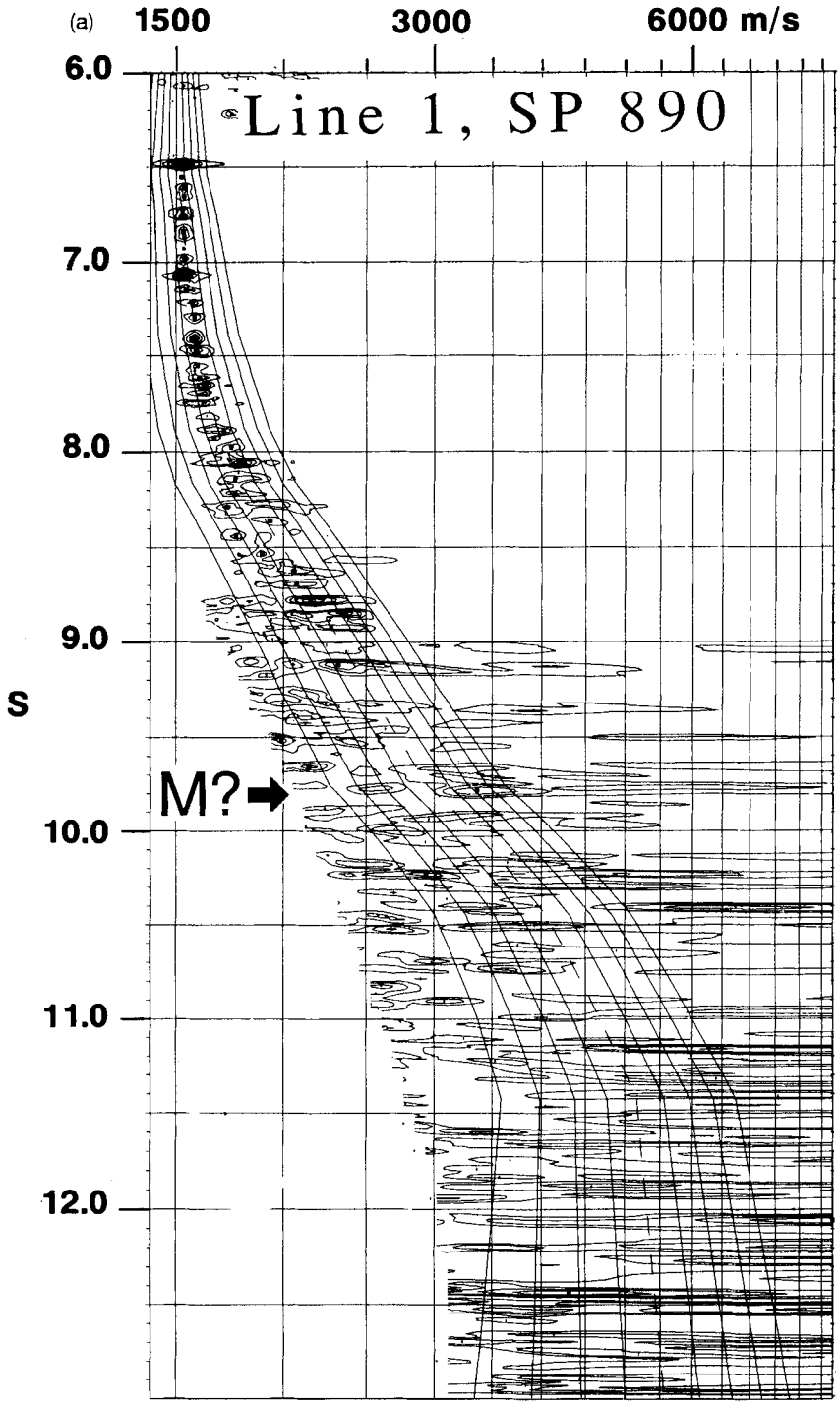

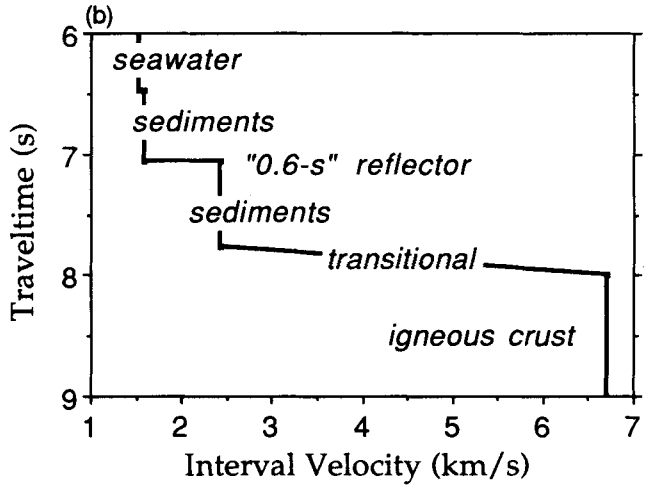

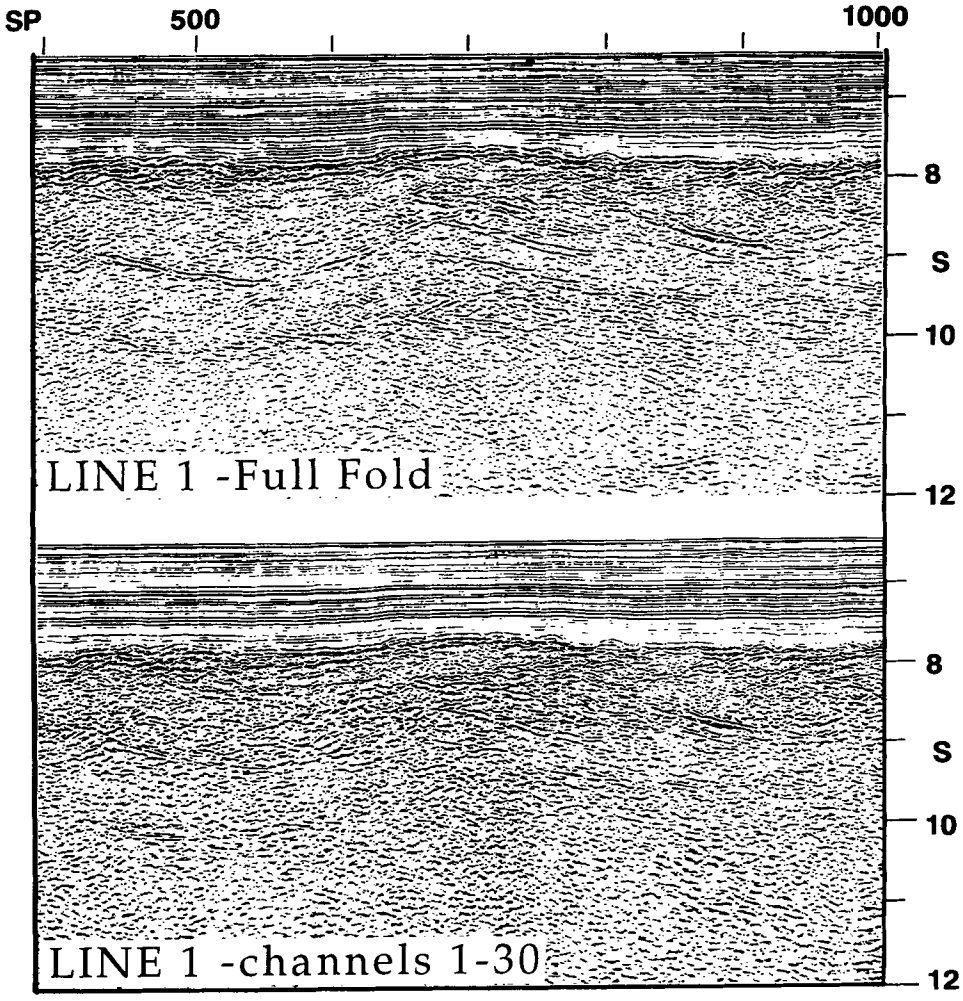

Figure 9. (a) Portion of Line 1 stacked section processed at full, 45 CMP fold. (b) As above but with first 30 channels (7.5 CMP fold) used in stack. The sections are finite-difference migrated.

Along most of the strike profiles, this surface, once migrated, is surprisingly smooth with a broad relief of no more than 300 m. Its relief becomes more extreme on the dip profiles, reaching a maximum of 1700 m.

One of the most surprising results of the BIRPS survey is the great variation in crustal structure observed along the 113 km long segment of the Early Cretaceous Mid-Atlantic ridge. Previous reflection programmes have actually documented *less* variation over lines spaced many 10's of kilometres apart. Variation on the profiles is expressed in the internal structure of the igneous crust, the direction of dip for dipping reflections on the flow profiles, and the structural relief developed at the top of the basement. The most marked variation is in the rapid change in the structure of the top of basement progressing from Lines 7 through 11. Beginning on Line 8 and continuing southward, the relief increases to 1700 m and defines a 26 km wide 'valley' (Line 10, SP 420-920, Fig. 12) bordered by back-tilted basement ridges. The interior of the valley is cut by smaller basement blocks (e.g. Line 9, SP 170, Fig. 12) almost identical to those imaged on Lines 3–6 to the north. As noted above, this area occurs along a small-offset fracture zone or possible non-transform discontinuity. This variation rapidly dies out along strike—by the time we reach the west end of Line 11 (Fig. 12), the top of basement is only gently undulating without any prominent structure, and the igneous crust appears relatively structureless internally.

Intracrustal dipping reflections parallel to the ridge axis

The spreading axis was surveyed approximately along-axis by two strike lines (Lines 1 and 2, 113 and 43 km long respectively). Across the northern portion of Lines 1 and 2, concordant bands of subhorizontal-to-dipping reflections appear between the top of basement and the base of coherent reflectivity. These bands contain some of the brightest reflections on any of the profiles and can be observed even at short offsets (i.e. with low CMP fold) (Fig. 9). The highest concentration occurs beneath a broad basement ridge between SP's 550 and 900 on Line 1 (Fig. 12). The migrated dip of the reflections, after removing the effect of the overlying sediment wedge, is 10–15°. The bands occur in bidirectional sets that criss-cross in places (e.g. below SP 680, Line 1, Fig. 12) suggesting that one of the sets may be reflecting from out of the plane of the section. This criss-crossing occurs on both migrated and

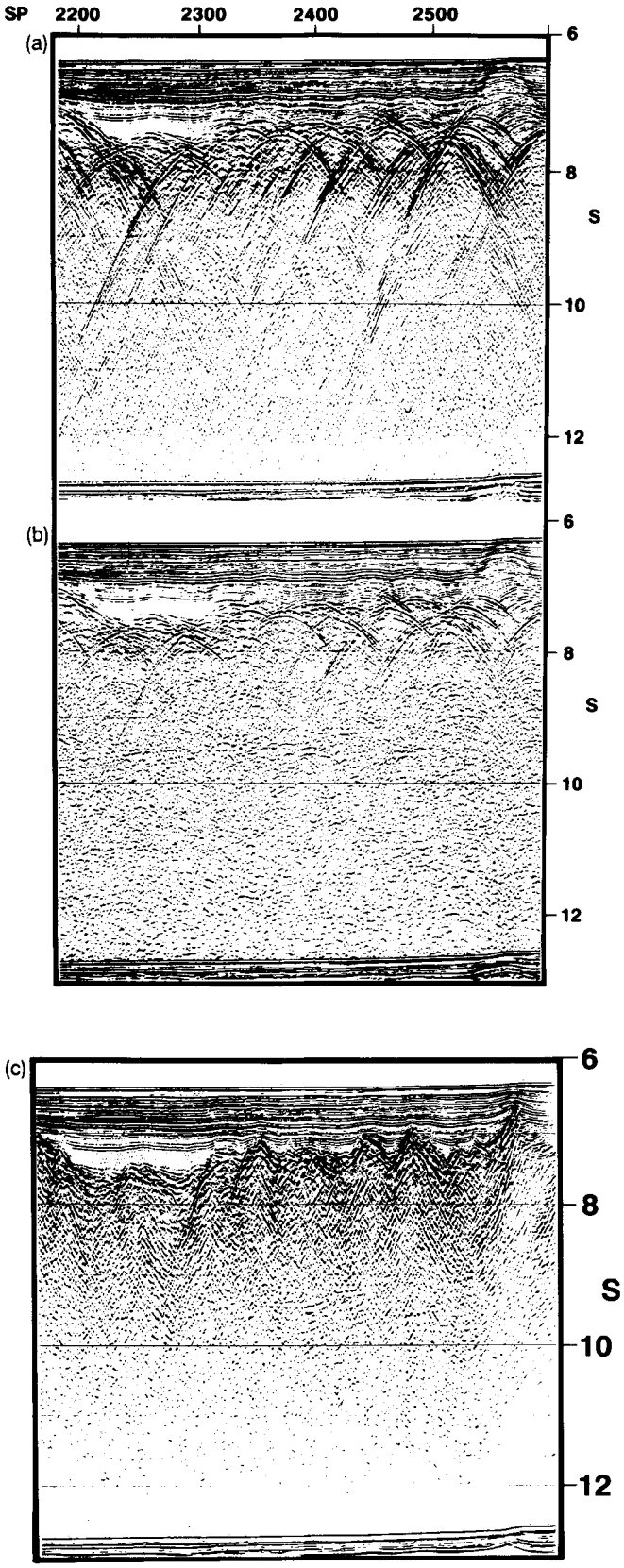

Figure 10. (a) Portion of Line 10 stack unmigrated with only frequency bandpass filters. (b) As in (a) but with frequency-wavenumber (f–k) filter designed to reduce contamination by diffraction from the top of the igneous crust ('D' in Fig. 12). Note the improved expression of the Moho reflection (9.5 s) by reducing diffracted noise by f–k filter prior to migration. (c) Stolt migration (1.55 km s^{-1}), which just collapses the diffraction hyperbolae of (a) but without an f–k filter. Note here the poor expression of the Moho reflection when no pre-migration f–k filter is used.

unmigrated versions of the sections. The 30-channel stack (Fig. 9b) appears to preferentially image the south-dipping reflectors which suggests that these may be nearer to being in the plane of the section. The vertical extent of the dipping bands is limited below by a prominent, flat-to-subhorizontal reflection ('M', Fig. 12). On the basis of modelling wide-angle arrivals recorded by ocean-bottom seismometers during a later cruise (Henstock *et al.* 1994; White *et al.* 1994), 'M' can be identified in some places as a near-normal incidence reflection from the Moho discontinuity. Some reflections dip entirely through the interval between the top of basement and 'M', but interact geometrically with 'M' in two ways. In places (Line 1 SP 600–700), the relationship is abrupt truncation of dipping reflections by 'M' as at an angular unconformity. Elsewhere (Line 1, SP 800–1200) the relationship is less clear as dipping reflections appear to approach 'M' asymptotically and possibly merge with it. Dipping crustal reflections consistently do not penetrate or extend below 'M'. Although individual dipping reflections can in places (Line 1, SP 700–800) be traced up to the top of basement, they are not usually associated with any offset of it or offset within the sedimentary section. Many reflections, or at least their brightest parts, appear to be confined to a level in the mid-crust (Line 1, SP 400–550, 1400–1700). Experiments with different migrations produced no significant change in these relationships. A contrasting reflectivity pattern emerges from the area near the southern ends of the two isochron profiles which is inferred to be somewhat anomalous from the magnetic data. This area is dominated by a major basement ridge, corresponding to the small-offset discontinuity (Fig. 1b), that widens to the east and has a more horizontal intracrustal reflector pattern than that further north. On both Lines 1 (SP 2000) and 2 (SP 200), the southern edge of the ridge is marked by a straight reflection dipping 33° to the south-east that appears to penetrate the crust (Fig. 12).

Intracrustal dipping reflections perpendicular to the ridge axis

We recorded nine dip profiles (Line 3 18 km, Lines 4–9 40 km, and Lines 10–11 80 km) which intersect the two strike profiles (Figs 1b, 12 and 13). The sections are dominated by dipping reflectors inclined either to the west or east, although events dipping westward towards the spreading axis are most prominent and common. Only west-dipping reflections correlate strongly with structural relief developed on the top of basement. The predominantly west-dipping fabric is corroborated by f–k spectra (Fig. 14) computed for the section between 8.0 s and 'M' which show a west-dipping bias after a water-velocity migration has been applied in order to suppress scattering from the top of basement. The top-basement reflector on the northern flow profiles (Lines 3–7) is interrupted by a series of short-wavelength pyramidal basement blocks (Fig. 12) that

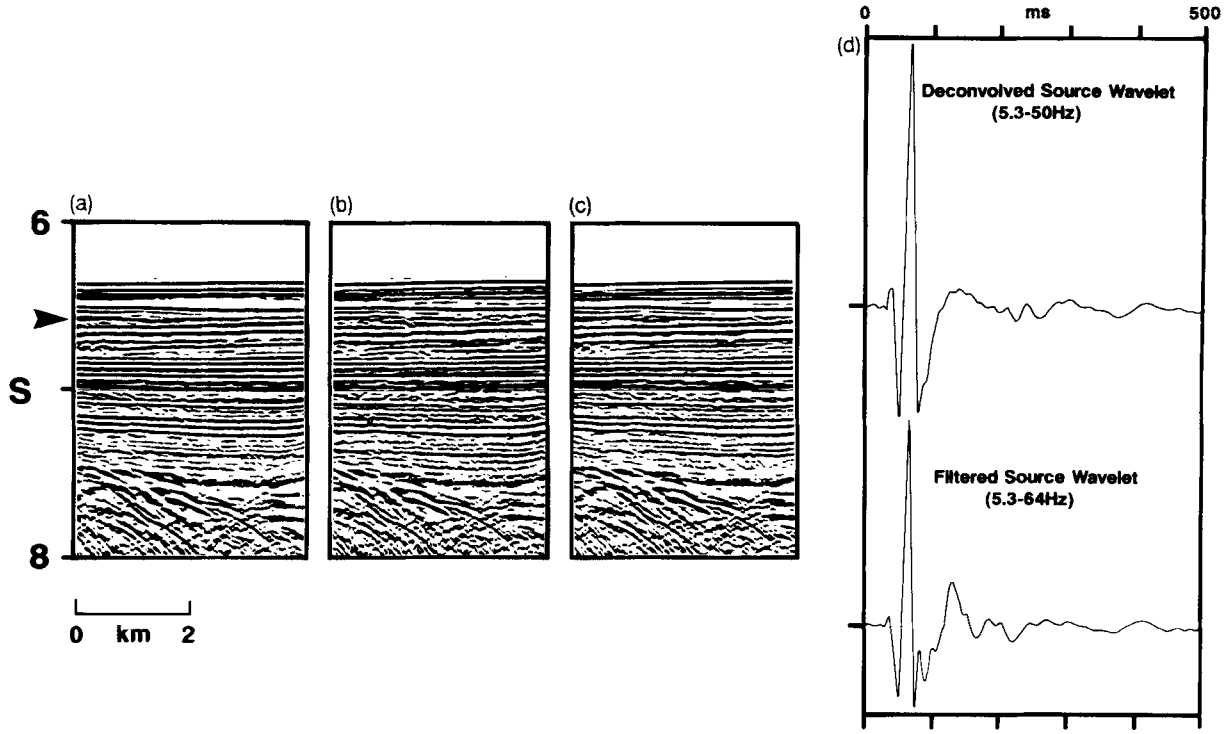

Figure 11. (a) Small portion of eastern end of Line 11 stacked section without deconvolution filter, (b) with a predictive deconvolution (32 ms, gap; 244 ms operator length), and (c) as in (b) but with operator length shortened to 144 ms; used for filtering the sediment portion of all post-stack data. See also Table 2. (d) Deconvolved (using parameters in c), bandpass filtered model of source wavelet (see Fig. 2) compared with filtered model source wavelet. Note increased peak-to-peak amplitude and retained low-frequency signal in deconvolved wavelet.

develop progressively southward. These basement blocks are often marked on their western flanks by steeply dipping (20–25°) reflections within the igneous crust (e.g. reflection 'W'). Although it appears to be possible to follow reflection 'W' with varying degrees of success across the entire set of dip lines (see arrows on western ends of Lines 4–11, Fig. 12), it is not clear whether we are looking at a single continuous surface striking parallel to the ridge axis or multiple *en echelon* fault sets oriented slightly oblique to the ridge axis. Between some lines (e.g. Lines 6 and 7, Fig. 12) the position of the west-dipping reflection can vary by as much as a few kilometres.

West-dipping reflections such as 'W' when migrated penetrate much or all of the igneous crust and appear in places to truncate and possibly offset flat-lying reflections within the igneous crust (e.g. 'B' Fig. 12). Marked variation in dipping reflectors is expressed across consecutive lines as well as along any individual line. For example, on Lines 5–6 the most prominent west-dipping reflections appear on the western end of the sections, whereas similar events are best developed on the eastern ends of Lines 7–9. Furthermore, some reflections penetrate the entire crust while others extend no deeper than the mid-crust. Dipping reflections occur as isolated, individual events and not as bands as on the strike lines. These reflections are the brightest features on the dip profiles showing a character similar to dipping reflections on the strike profiles, especially when comparing the 30-channel stacks (*cf.* Figs 9 and 15). Like the shallower dipping reflections on the strike profiles, 'W' does not cut or extend beyond 'M', and remains planar or slightly convex upward upon migration (Fig. 15). The upward convexity may be an artefact of the bulge in the top of basement above the down-dip part of 'W' causing a slight velocity pull-up. Where the basement surface becomes rougher further south (Lines 7–9, Fig. 12), west-dipping reflections beneath the flanks of basement ridges are broken into uneven segments due to lateral velocity variations above.

West-dipping reflections often line up with small-displacement faults developed within the overlying sediments. This line-up is more obvious from the 30-channel stacks (Figs 15 and 16a, b) which have greater accuracy, particularly for dipping reflections that suffer more CMP smearing than horizontal reflections when stacked at full fold (Levin 1971). Displacement within the sediments increases with depth with offsets of ~20 m observed, which is reaching the limit of resolution (using Rayleigh criterion) for measured frequencies of about 40 Hz (Fig. 17). Fault planes defined within the sediments extend directly into crustal dipping reflections such as 'W' at the edges of the pyramidal basement blocks. The association of dipping reflections with offsets defined in the sediments, with offsets on top of basement, and with truncations of intracrustal reflectors implies that these reflections are from faults. A detailed study (Figs 16a, b, d) shows that the sense of offset in the sediments is usually normal, down to the west. Sedimentary layers above the prominent '0.6 s' reflection are generally unaffected by faulting. Although east-dipping synthetic and/or antithetic faults within the sediments do occur, they are not directly associated with dipping reflections in the igneous crust (Fig. 16c). The hanging-wall

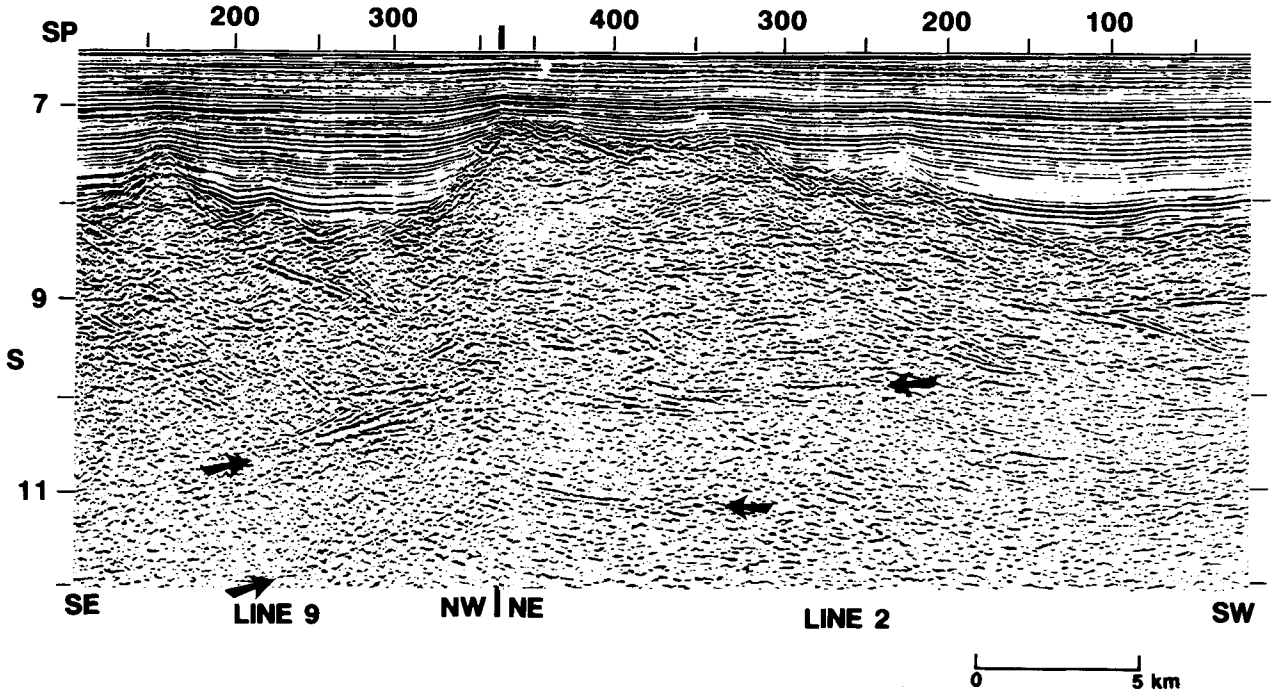

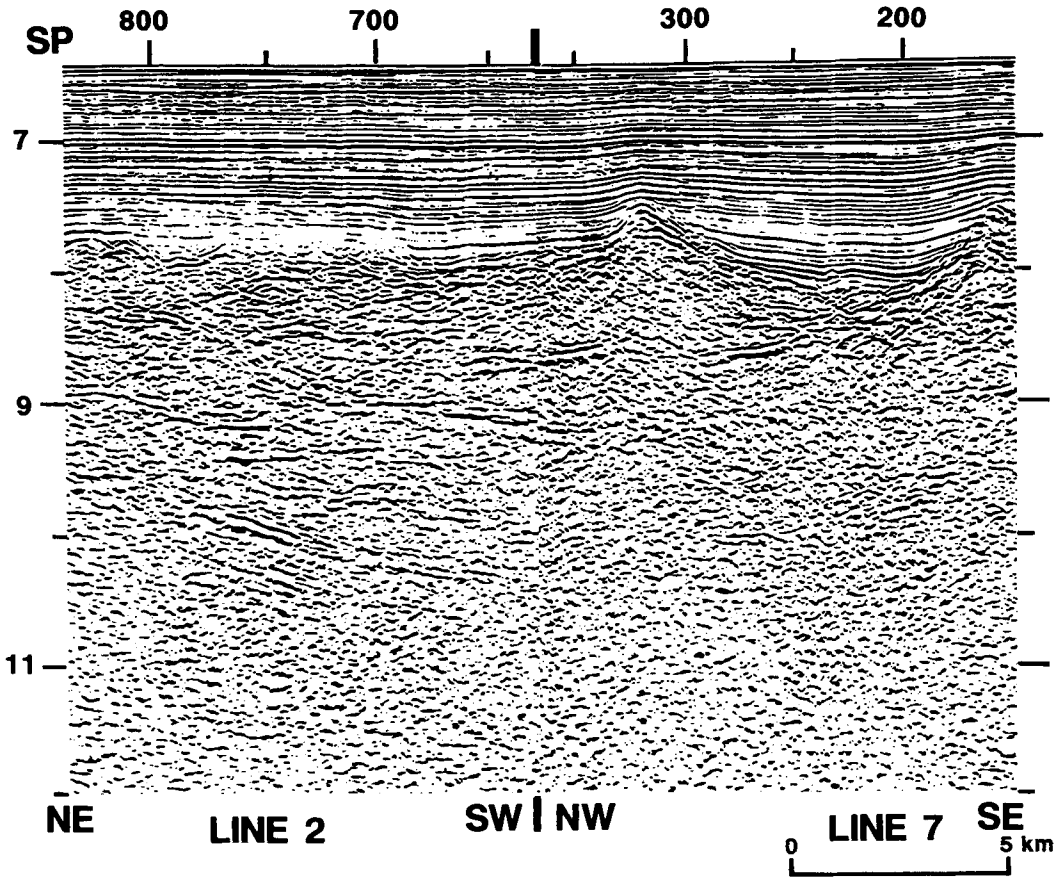

Figure 13. Three sets of intersecting lines tied to each other (see Fig. 1 for location of tie points).

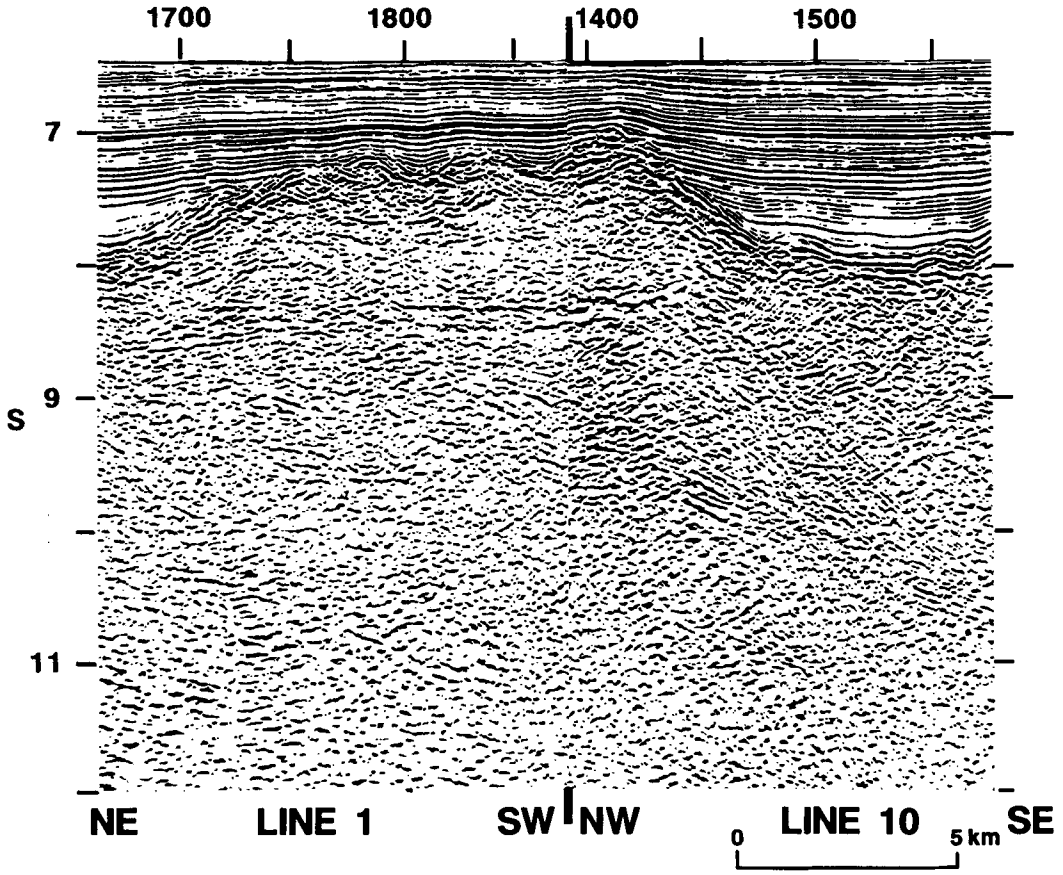

Figure 13. (*Continued.*)

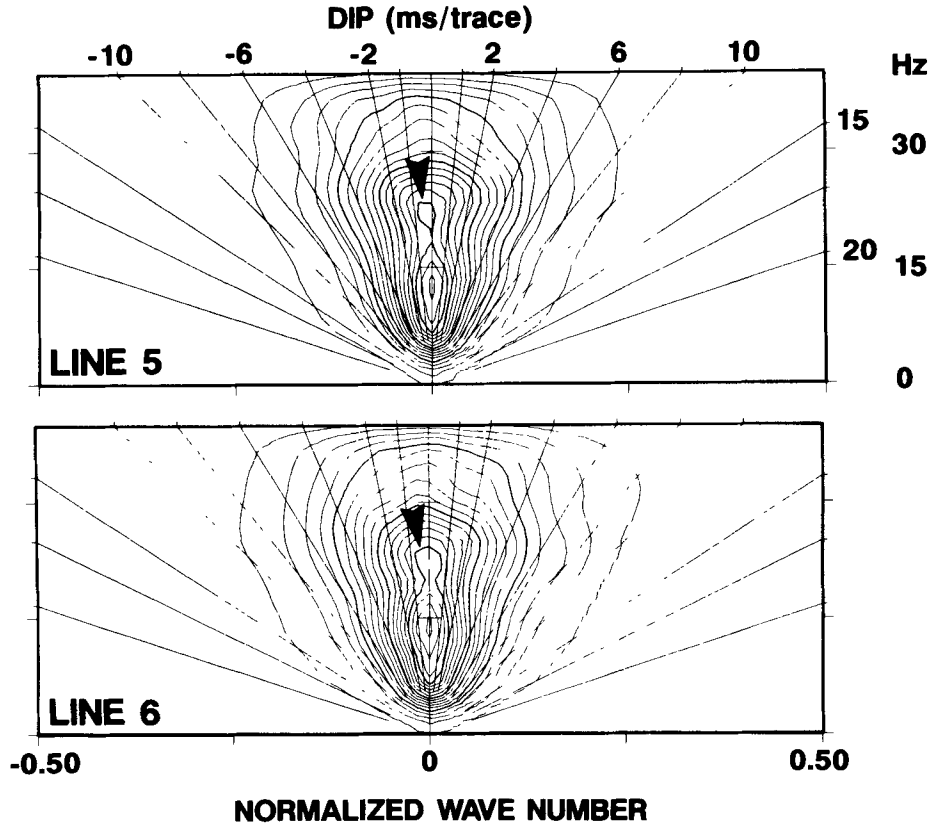

Figure 14. Frequency-wavenumber spectra computed for the igneous crust portion (8–10 s) of Lines 5 and 6 after a 1.55 km s^{-1} Stolt migration (to just collapse diffraction hyperbolae) but with no filters or amplitude balancing. Note bias for west-dipping events within crust on both lines regardless of shooting direction.

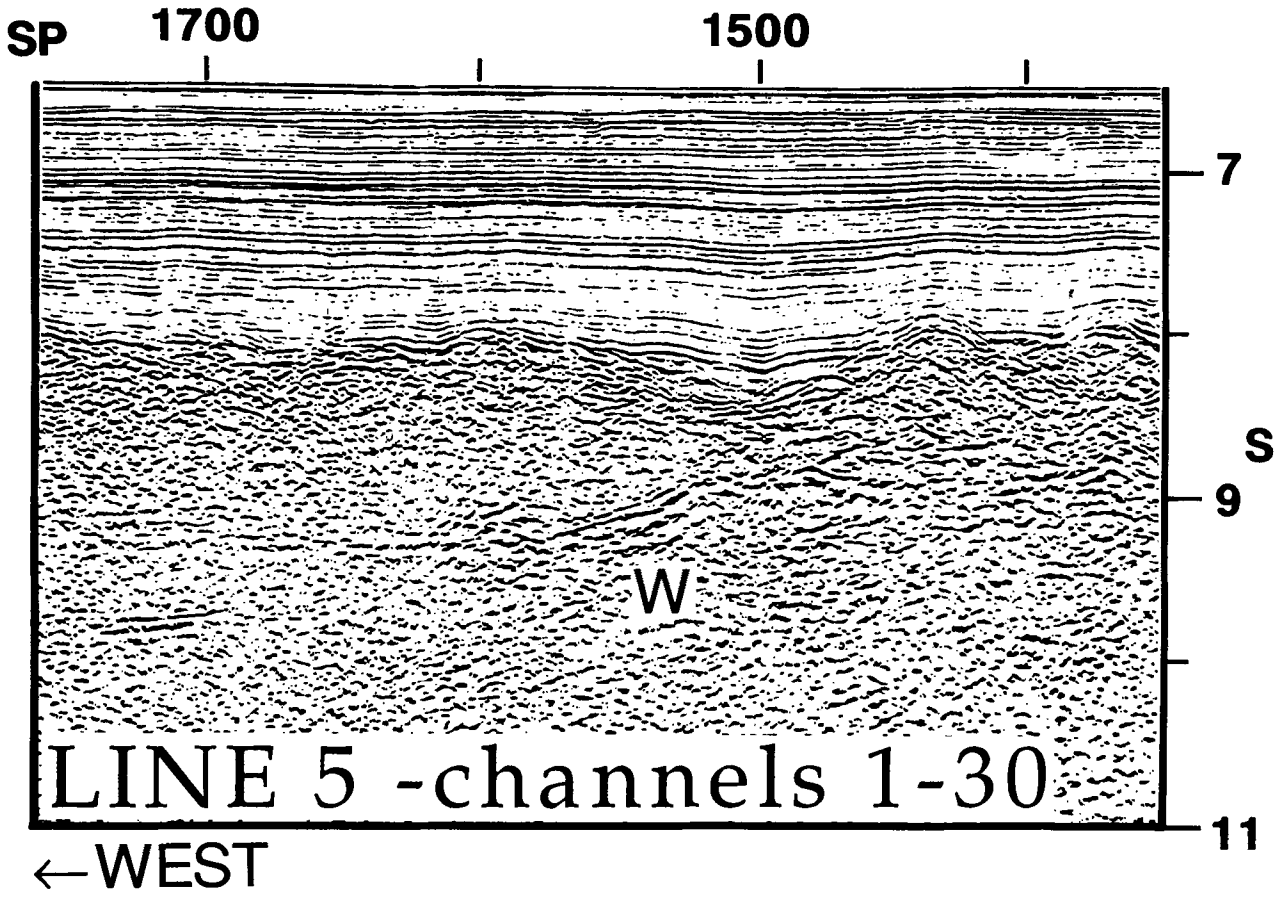

Figure 15. Migrated stack using first 30 channels of streamer of the western portion of Line 5, which improves the accuracy of crustal events (e.g. 'W'), but reduces overall s/n deeper. Processing is otherwise identical to that used for Line 5 in Fig. 12.

portions of the faults are situated over depressions on the top of igneous basement. Evidence of minor reverse motion is sometimes observed in the sediments above the western edge of these depressions which, in analogy to growth fault systems in deltaic sequences, may be related to localized compression at the 'toe' of the hanging-wall block (White, Jackson & McKenzie 1986).

Lines 3–7, which traverse a 16 km long segment of the ridge, show a similar structure for the top of the basement and the overlying sediments; however, the higher-amplitude dipping structures within the igneous crust appear to alternate from line to line, even though the spacing is only 4 km (Fig. 12). For example, on Line 5 'W' is strongly developed as a west-dipping high-amplitude reflection. 'W' is also present on Line 6 but with much less amplitude and coherency; the most prominent event on Line 6 is actually east-dipping ('E', Fig. 12). On the western end of Line 7, the brightest reflection is again west-dipping like on Line 5. Although it is tempting immediately to attribute geologic significance to this variation, we are concerned about possible bias introduced by the direction of shooting. A bias for imaging steeply dipping structure that reflects from out of the plane of the section has sometimes been observed on 3-D surveys particularly over complex structure (Beasley & Mobley 1988; Egan, Dingwall & Kapoor 1991). Over the western parts of Lines 5–8, odd-numbered flow profiles, which were shot east to west, tend to show a preference for west-dipping reflections (e.g. 'W') whereas even-numbered flow profiles shot the other way, tend to show east-dipping reflections (e.g. 'E'). This bias is weakly expressed in that it appears to affect only the western portion of the profiles. Although for moderately dipping reflectors (i.e. $20° \pm 5°$) at the depths involved in our study (6.5–9.0 km) the hyperbolic traveltime function in the shot domain will vary significantly depending on the direction of shooting (Fig. 18), this bias should disappear once the traces have been CMP sorted (Cressman 1968).

In order to understand better the dipping reflection ray paths, we studied their behaviour starting with the shot records, through to CMP sort, and using range-limited stacks (Fig. 19). The asymmetric traveltime curves of west-dipping reflections appear as expected for dipping reflectors imaged with the ship steaming in (Line 5) or against (Line 6) the dip direction (Fig. 19a). As expected, after CMP sort (Fig. 19b) the traveltime curves are symmetric about the zero-offset axis and show no unusual NMO. Further, 'W' displays a simple amplitude-versus-offset behaviour, with brightness and coherency dying gradually over the far offsets (Fig. 19c). Thus, we believe the west-dipping reflections are in-plane and not side-swipe or diffractions. The traveltime behaviour of east-dipping reflections is less clear. Reflection 'E' on Line 6 appears to be a mix of horizontal and east-dipping elements on the migrated section (Fig. 12), while on shot records no single

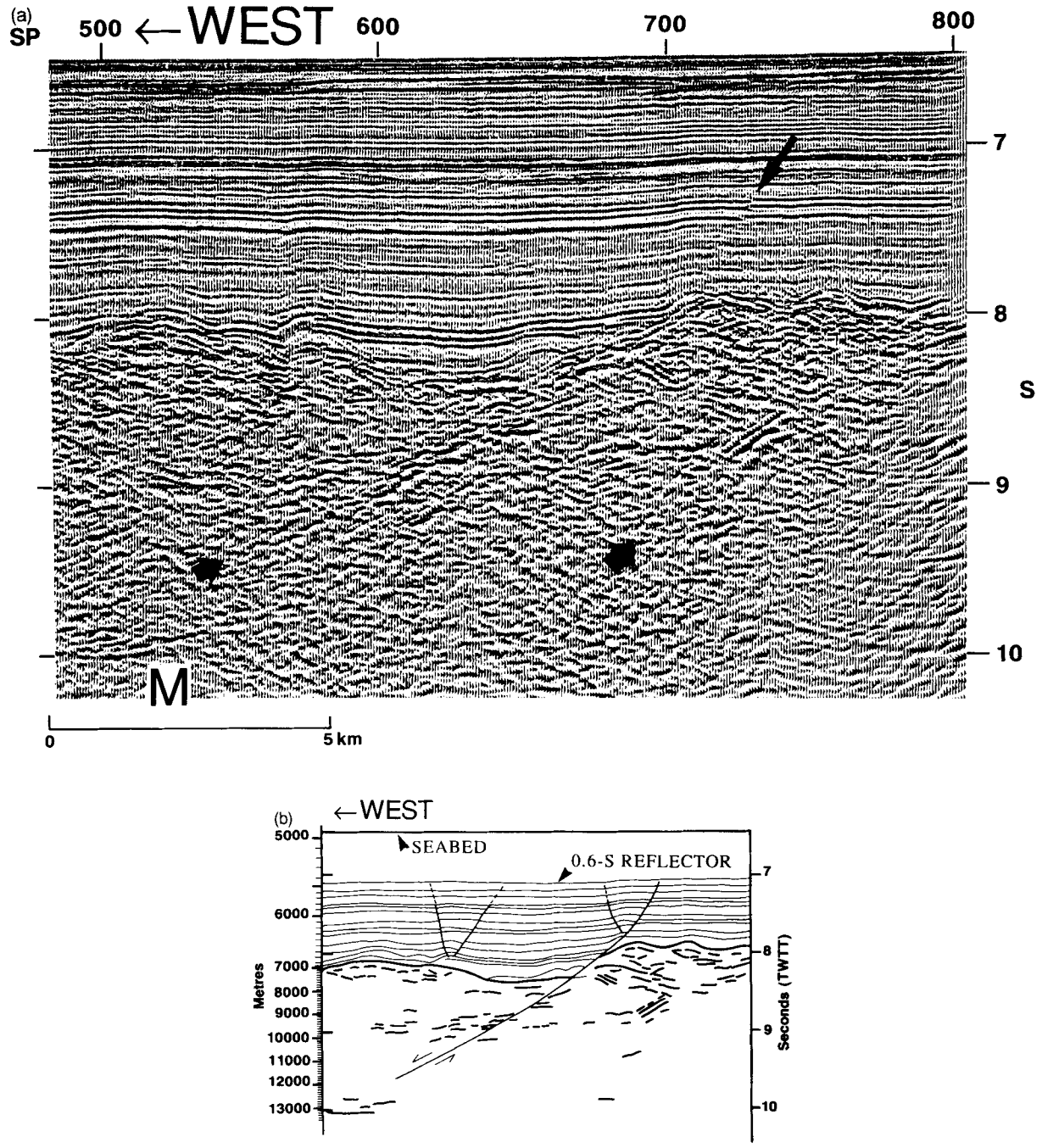

Figure 16. Detailed interpretation of normal faults in igneous crust extending into small-displacement faults in the sediments. (a) Line 4, stacked with first 30 channels and finite-difference migrated (as in Fig. 12). 'M' is interpreted Moho reflection. Displayed with variable area and wiggle trace. (b) Line-drawing interpretation of (a) after depth conversion (using function in Fig. 8b). (c) Migrated full-fold stack of Line 3 showing normal faults (arrows) on either side of basement ridge. (d) Portion of post-stack depth migration of Line 5 showing continuation of normal fault from basement into sediments, vertical exaggeration 2.5:1.

event dominates. It is thus possible that the east-dipping reflections come from more complex structure out of plane.

The two orthogonal intersections of the strike and dip lines give us a limited amount of cross-line control on reflection geometry. Unfortunately, the prominent 'W' reflection lies too far to the west of Line 1 to be correlated across; however, the shallow-dipping reflections on Line 7 tie clearly to a horizontal reflection packet on Line 2 at about 8.6 s (Fig. 13). Conversely, some of the prominent horizontal dip-line reflections (e.g. 'B') within the crust can be correlated to individual dipping events composing the reflective bands on the strike lines (*cf.* Lines 1 and 5, Fig. 12).

Moho and general intracrustal reflectivity

The expression of the Moho discontinuity ('M') varies considerably, being very well developed as a reflection in some areas and totally absent in others. This is surprising

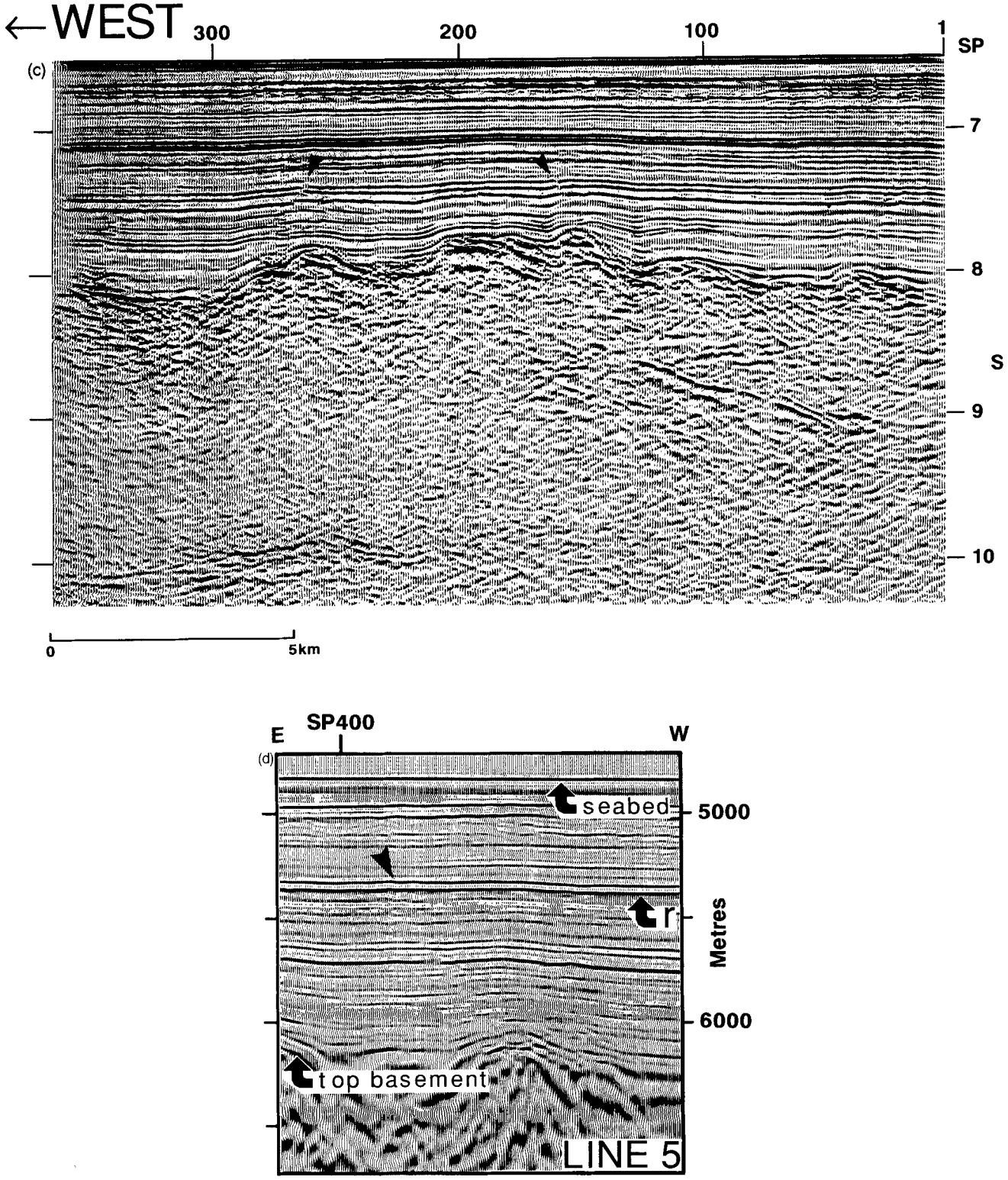

Figure 16. (*Continued.*)

because shooting conditions and equipment operation were uniformly good throughout the programme, and because the survey was concentrated over a relatively small area. On the strike profiles, 'M' is expressed as isolated segments of simple subhorizontal reflections with a maximum length of ~7 km (Fig. 12). The continuity and frequency content (Fig. 17) of Moho reflections are essentially the same as that of overlying crustal reflections. Where the amplitude and coherency of 'M' are high, it shows a well-defined semblance peak at rms velocities of $3350 \pm 50\ m\ s^{-1}$ (Fig. 8a). Where a prominent Moho reflection is unclear or absent, a 'boundary' at 9.5–10 s still appears to be definable

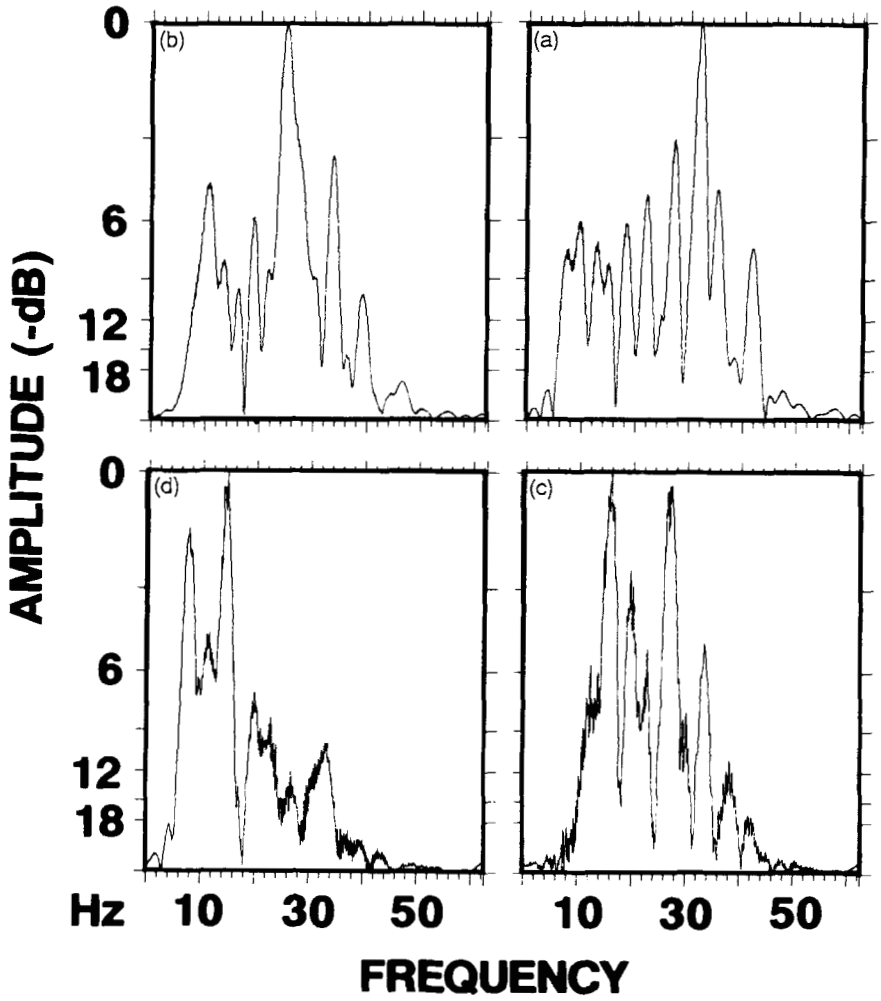

Figure 17. Frequency spectra for SP 835-908, Line 1 computed from 30-channel stack (which reduces the NMO shift in frequency) after a Stolt 1.55 km s^{-1} migration for time interval corresponding to (a) sediments between sea-floor and '0.6 s' reflector, (b) sediments between '0.6 s' reflector and top of basement, (c) upper crust (8.3–8.8 s), and (d) uppermost mantle (11–11.5 s).

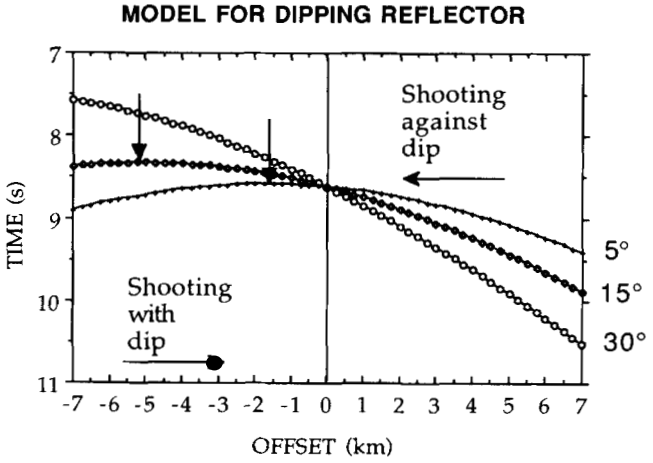

Figure 18. Model-shot record traveltime curves (using dip-move-out equation: Sheriff & Geldart 1982) for reflectors dipping at angles showing using a smoothed version fo the velocity model given in Fig. 8(b) depending on the direction of shooting. Vertical arrows give axes of symmetry (i.e. given by the line $x = -2h \sin(\xi)$, where x is offset from the shot point, h is the distance normal to the dipping reflector, and ξ is the dip). For 30° reflector, the axis is off the record to the left. Compare with Fig. 19.

on the basis of a change from coherent reflectivity above 'M' to a lack thereof below, especially on the dip lines. Compared to the strike lines, coherent Moho reflections on the dip profiles are less well expressed or simply absent. On some of the dip profiles (especially Lines 6–7) a level of horizontal reflections occurs at 9.5–9.6 s (Fig. 12). These are parallel to, but distinct from, the Moho reflection (e.g. middle Line 6). In other areas across the survey (e.g. east Lines 10–11), the interior of the igneous crust appears to be dominated by chaotic structure. The most prominent lower crustal reflection appears beneath the western flank of the rift valley on Line 10 and ties to a bright horizontal reflection ('m') beneath the strike lines (Fig. 13). Modelling wide-angle arrivals (Henstock *et al.* 1994) indicates that this reflection is not the Moho but coincides with the top of a layer with a velocity beginning at 7.5 km s^{-1}.

During the survey, we extended the southernmost two dip lines (10–11) an additional 40 km beyond the block-faulted area observed to the west. Over this part of the survey, igneous crust is more or less incoherent internally but shows a series of reflections at about 9.5 s extending for almost 30 km along the lines (Fig. 20) interpreted as Moho. Their appearance, however, is distinct from Moho reflections

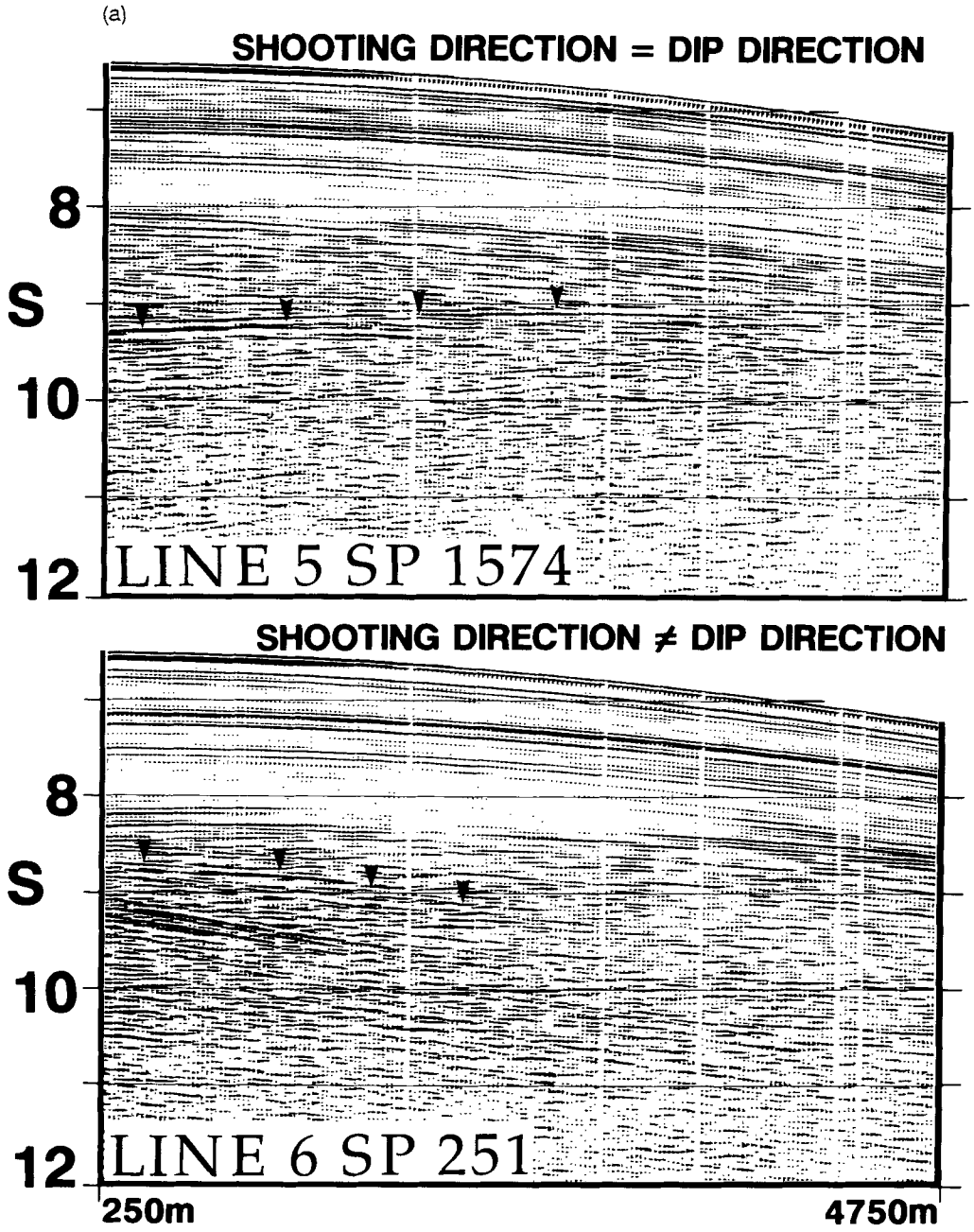

Figure 19. (a) Shot records from the western portion of Lines 5 and 6 over reflection 'W' (SP's (1)574 and 251). Traveltime of 'W', noted by arrows, is as expected for the shooting direction (*cf.* Fig. 18). (b) CMP gathers showing 'W' (arrows) from Lines 5 and 6 corresponding to shot gathers in (a) (i.e. for different directions of shooting). (c) Stack panels for Line 5 over 'W' (just below 9 s) stacked with the range of offset indicated. Note smearing of wavelets at far offsets.

elsewhere across the survey. Here, the Moho reflection consists of short, discontinuous segments usually no more than a few kilometres long. Furthermore, the degree of roughness on the top of basement, which determines the level of scattered energy from diffractions, appears to control the lucidity of the Moho reflection. For example, where the Moho is poorly imaged (Line 10, Fig. 20a), the top of basement is very rough, but where the Moho is better expressed (Line 11, Fig. 20b), this surface is much smoother. As discussed above, a robust f–k filter applied post-stack was required to eliminate this effect since migration alone was not sufficient to suppress the scattered energy (Fig. 10b). Regardless of the severity of scattering, the Moho reflection shows a strong peak in reflected amplitude and marks the base of prominent reflectivity on either section (Fig. 20c). The variation in the expression of Moho reflectivity across this part of the survey can be explained by the varying degree of roughness on top of basement and, in this case, may thus be geologically insignificant.

Upper-mantle reflectivity

In most places over the survey area, the sections lack coherent reflections below the level of the Moho.

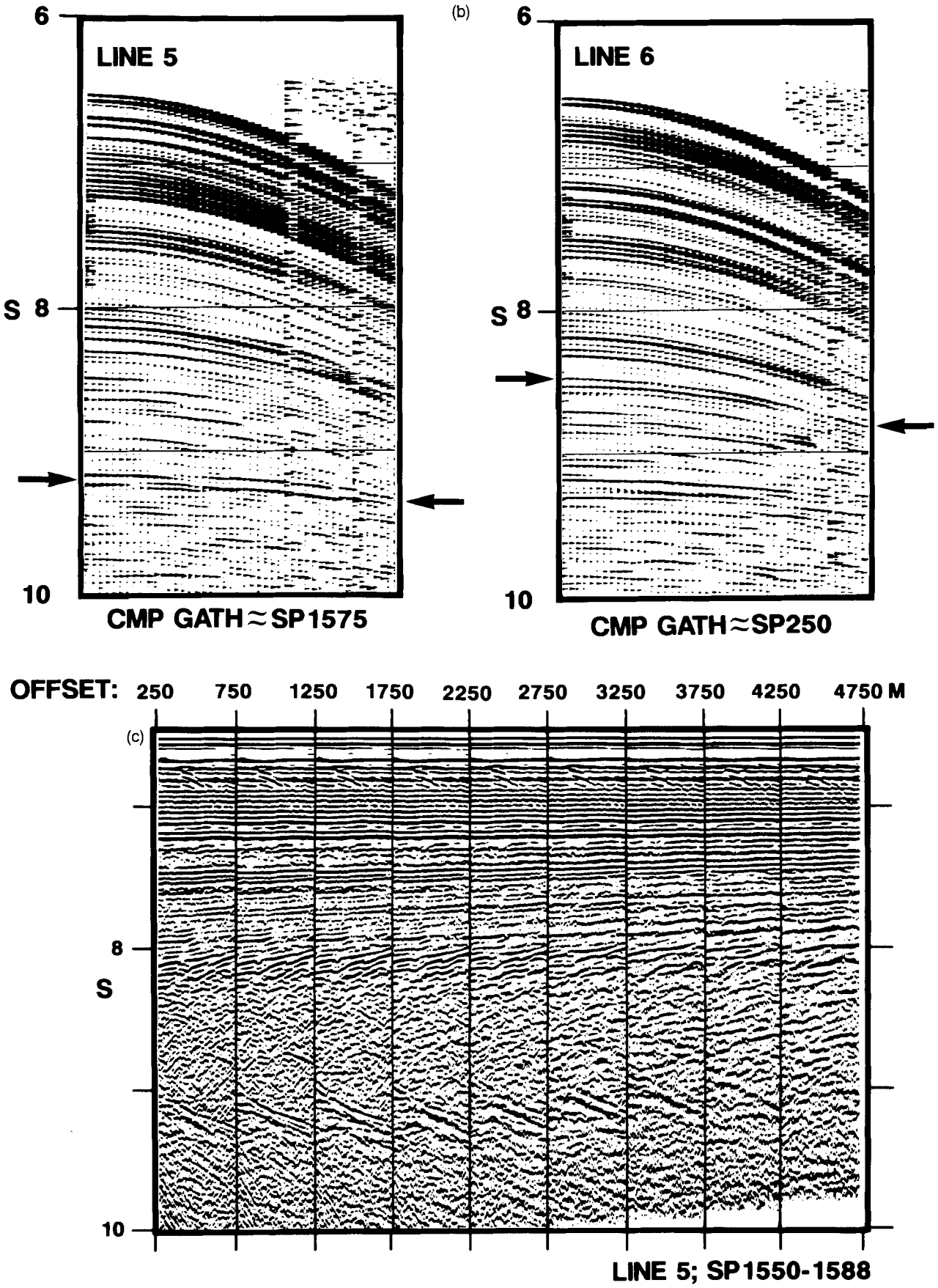

Figure 19. (*Continued.*)

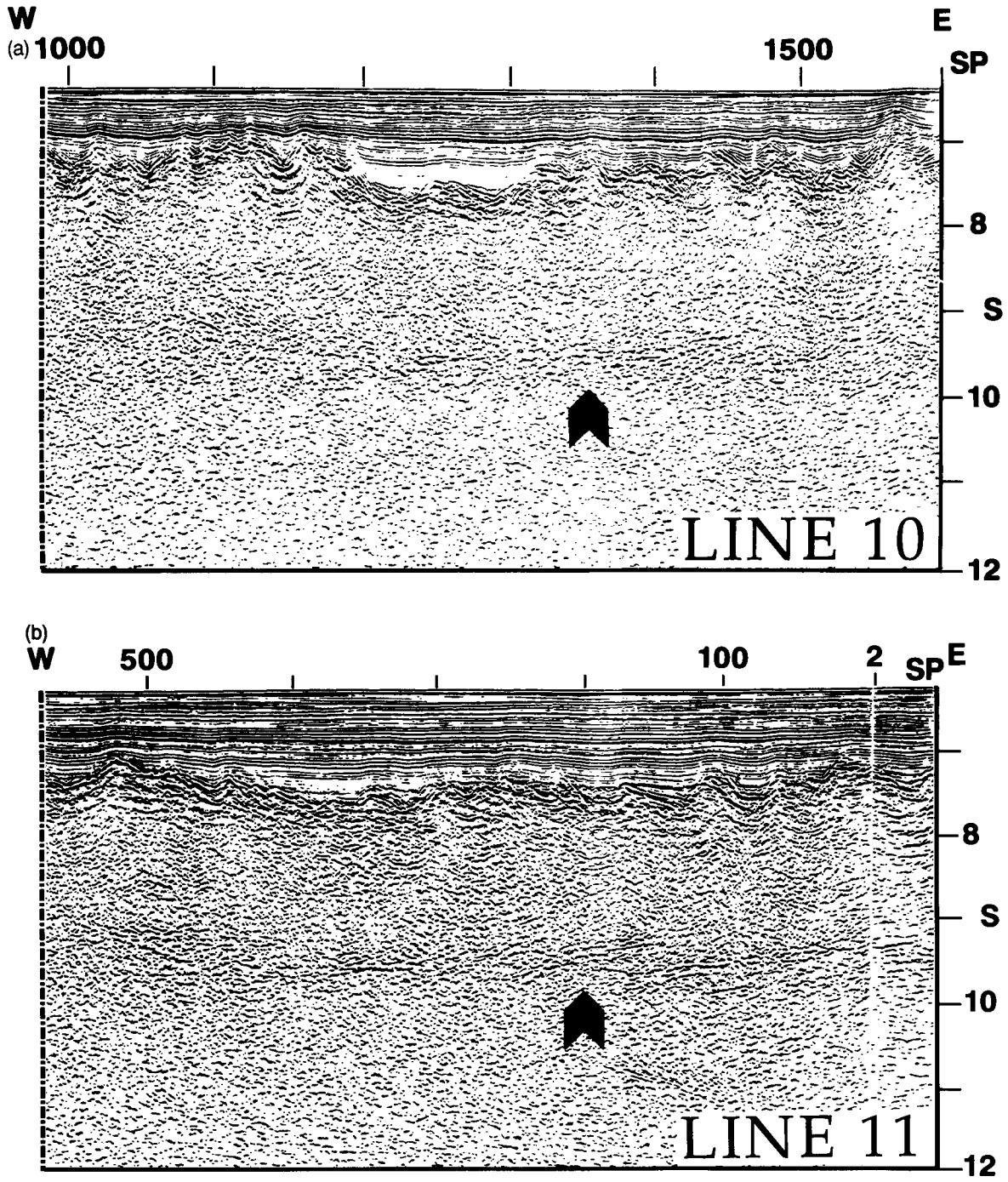

Figure 20. Eastern portion of Line 10 (a) and 11 (b) processed as in Fig. 12. Arrow indicates interpreted Moho reflection. (c) amplitude decay curves computed from raw unfiltered and non-amplitude balanced migrated CMP data for central portions of Lines 10 and 11 shown. M_1 is the first seabed multiple.

Nevertheless, a general division between the crust and upper mantle is implied from the clear decrease in reflected amplitude beneath the crust (Fig. 20c) on most of the profiles regardless of whether or not the Moho is actually expressed as a coherent reflection. This contrast provides further evidence that the uppermost mantle beneath the oceans is homogeneous on the scale of the seismic wavelength (500–800 m) relative to the crust. Several exceptions, however, do exist on our profiles. Along parts of Lines 1 and 2 (Fig. 12), a discontinuous band of low-frequency (Fig. 17) events begins below 10.0 s in the upper-mantle portion of the section. Such events occur only on the strike lines and are distinct in character from the very weak wrap-around multiples sometimes observed (Fig. 7a). The most prominent of these appears on Line 2 (Fig. 12, 'X' and 'Y') as a gently dipping pair of reflections that steepen upward but do not continue above the level of the Moho. Where correlation onto dip lines is possible, these reflections tie to the steeply east-dipping sub-Moho reflections on Lines 9–10 beneath the flank of a major

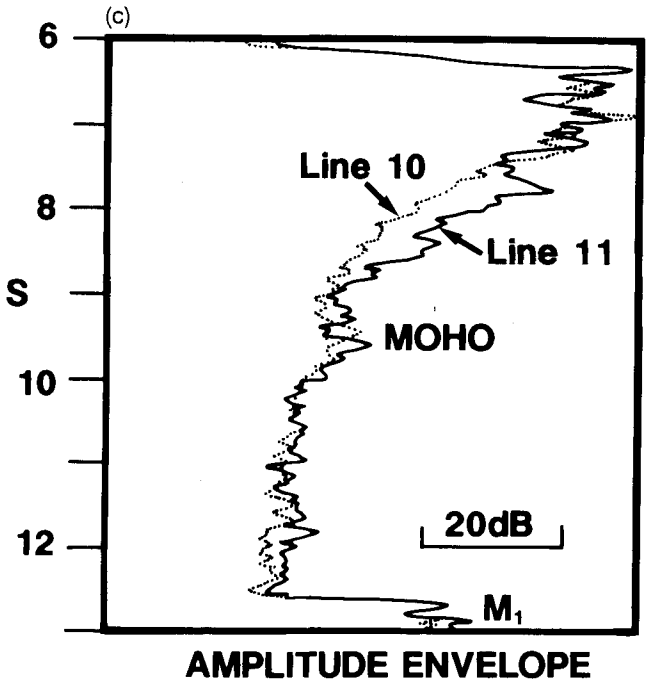

Figure 20. (*Continued.*)

basement ridge (Fig. 13). Elsewhere on the dip profiles, clear reflections arriving at mantle traveltimes are absent except beneath a portion of Line 11 where a pair of very steeply dipping (~35°) events occurs just below the Moho reflection (Fig. 13). The westward dip of these reflections is opposite to that observed along strike on Lines 9–10. Interpretation of the mantle events observed on the profiles is difficult since they cannot be traced into the crust or be uniquely related to any particular basement feature. Dipping upper-mantle events have generally not been observed elsewhere on reflection records from the Atlantic although have been reported from the Blake Spur fracture zone area (Minshull *et al.* 1991; Morris *et al.* 1993).

DISCUSSION: DIPPING REFLECTIONS IN THE IGNEOUS CRUST

An emerging view from recent seismic experiments is that the velocity structure of ocean crust is heterogeneous on a scale of a few kilometres at least in the upper crust (e.g. Swift & Stephen 1989). A principal result of this survey is that for both isochron and flow profiles, a complex dipping fabric for the igneous crust dominates a horizontal one. Although some of the dip lines (6–7) show a horizontal mid-crustal reflector, in general we see little evidence for a systematic division of oceanic igneous crust as discussed by Mutter *et al.* (1985) for similar-age crust on the conjugate side of the North Atlatnic. A discontinuous reflection interpreted as the Moho is the only persistent horizontal feature below the top of basement. The scale of variation in the Moho reflection seems large compared to the small size of the survey area itself. Small-scale varations in the amplitude and coherency of the Moho reflection observed on the opposite side of the North Atlantic (NAT Study Group 1985) have been related to similar-scale petrographic variations observed at the base of the crust in ophiolites (Collins, Brocher & Karson 1986). However, we have shown that at least some of the variation appearing on the BIRPS sections (e.g. east ends of Lines 10–11) is due to a varying severity of scattering from the top of igneous basement.

Dipping reflections on dip profiles: faults

One of the major interpretation issues for these data is the origin of dipping reflections within the igneous crust. Various patterns of dipping intracrustal reflections have been observed from other reflection data sets on both sides of the Atlantic, but line spacings were always too wide to visualize such features in three (or 'two and a half') dimensions. Previous workers have interpreted dipping reflections as fault planes, traces of extinct magma chambers originating at or near the ridge crest, or intruded basaltic sills (Mutter *et al.* 1985; McCarthy *et al.* 1988; White *et al.* 1990; Banda *et al.* 1992; Sinton & Detrick 1992). Previous fault interpretations were unable to demonstrate conclusively consistent offset of horizontal markers (McCarthy *et al.* 1988; Banda *et al.* 1992). On the other hand, the BIRPS dip lines show dipping reflections that clearly offset the top of igneous basement forming distinct ridges, reminiscent of a block-faulted 'basin and range'. The fault orientation is dominantly toward the Early Cretaceous spreading ridge although reflections inclined in the opposite direction are also observed; the latter appear not to be associated with offset within the igenous basement, on the top of basement, or in the overlying sediments. We have cautiously approached interpretation of the observed alternation of direction in dominant reflection dip on the dip lines. Alternation of the direction of fault dip with respect to the position of the spreading centre has been associated with either a fast-spreading rate (Carbotte & Macdonald 1990) or oblique spreading (Macdonald *et al.* 1988; Dauteuil & Brun 1993). Because the Early Cretaceous North Atlantic was a slow-spreading system that opened normal to the ridge axis (White 1984), neither of these explanations seems applicable for our observations. Further profiling at a much closer line spacing will be required to understand the observed alternation.

Microearthquake studies over the active Mid-Atlantic ridge indicate that brittle failure occurs as deep as 8 km below the ridge crest (Toomey, Soloman & Purdy 1988). This observation and results from rheological modelling of oceanic lithosphere (Chen & Morgan 1990; Phipps Morgan & Chen 1993), which indicate that much or all of the oceanic crust deforms brittly, are consistent with our interpretation of planar faults such as 'W' penetrating the igneous crust. The varying depths of penetration observed for interpreted fault-plane reflections on the dip lines may be related to the variable depth of crustal isotherms at the ridge that would cause the depth of the brittle/ductile transition to vary (Harper 1985; Toomey *et al.* 1988). The relationship observed in this study between dipping fault-plane reflections and tilted fault blocks developed on the top of igneous basement is the clearest yet found by deep-reflection studies of ocean crust. The 'preservation' of this relationship in Early Cretaceous crust is consistent with the

suggestion by Kong *et al.* (1988) that the active faulting at the ridge crest rapidly dies out as crust spreads away from the ridge. Banda *et al.* (1992) also observed basement blocks or ridges associated with planar dipping reflections in Cretaceous-age ocean crust on single lines west of the Canary Islands. Field studies of the Lizard ophiolite in England, which is analogous to the slow-spreading Early Cretaceous North Atlantic, document normal faults that cut the entire thickness of the igneous crust and that formed shortly after the construction of the crust (i.e. probably at or near the original ridge axis) (Roberts *et al.* 1993).

One possible difficulty with a normal fault interpretation for the west-dipping reflections on the flow profiles is that their dip falls far outside the usual 55°–65° range predicted for brittle failure when principal stress directions are unchanged (Turcotte & Schubert 1982). We believe the observed shallow dip of these reflections is structurally true, and not apparent, because the orientation of the dip lines is normal to magnetic-anomaly stripes and because no correlative dipping reflections occur on the strike lines near where they intersect. One explanation is that the observed dip is not original and the fault blocks may have slid toward the hanging wall along rotational faults (westward, towards the ridge) during their formation at the original spreading ridge. This rotation may have been accommodated deeper within the lithosphere along a low-angle detachment (Norrell & Harper 1988) analogous to those observed in metamorphic core complexes on the continents (Allmendinger *et al.* 1983). Such a mechanism has been proposed by Karson (1990) in order to explain evidence of tilted fault blocks and exhumation of lower crustal rocks in the footwalls at the modern-day Mid-Atlantic ridge (see Salisbury & Keen 1993 for review). Structural studies of the Josephine ophiolite, which represents a slow-to-intermediate-rate spreading centre, indicate that a significant amount of tilting (in this case, ~50°) of the igneous crust associated with normal faulting and magmatism is possible at or near the spreading centre (Alexander, Harper & Bowman 1993). Unequivocal evidence for crustal normal faulting is seen elsewhere in the North Atlantic in Middle Jurassic-age crust (Salisbury & Keen 1993).

Faulting history

The apparent continuation of the faults into the overlying sediments, as seen from our data, is a fairly new observation from ocean-crust reflection data. Differential sediment compaction across basement ridges may be the source of the faulting rather than reactivation of the basement faults; however, the lack of notable sediment thickness changes across the faults (Figs 16a, b, d) argues against mere compaction. Displacements can be traced from the edges of offset basement blocks up to the mid-Miocene '0.6 s' reflection (Figs 16a, b, d). Normal fault reactivation of basement faults would imply continued minor extension until the mid-Miocene and/or be related to the distal effects of uplift associated with the Cape Verde hot spot (Williams *et al.* 1990). Displacement of pre-mid-Miocene sediments implies that continued fault movement (or sediment consolidation) persisted for at least 120 Ma since initial formation at the ridge. A problem with a normal-fault reactivation interpretation is that studies of intra-oceanic plate seismicity imply that areas such as the Cape Verde abyssal plain are under compression and should undergo reverse or strike slip, but not normal, fault deformation (Sykes 1978; Wiens & Stein 1983). The stress system of the study area is likely to be affected by seismicity associated with the Canary Islands and the Cape Verde Islands. A magnitude-5.2 1989 event near the Canary Islands (Fig. 1a), which had a reported mainly reverse motion at 9 km depth within the lower part of the igneous crust, is fairly typical. Continuation of faults from oceanic basement directly into the overlying sediments has been clearly documented from reflection data for an intra-oceanic plate deformation zone in the Indian Ocean (reverse motion; Bull & Scrutton 1992) and for oceanic (or stretched continental?) crust in the Atlantic east of Nova Scotia (normal motion; Salisbury & Keen 1993).

Determination of the original age of the basement faults is not possible, but the observation that the faults do not cut or extend beyond the Moho reflection implies that they pre-date the formation of the Moho surface unless the Moho has acted as a detachment. We suggest that the faults developed initially at or near the spreading ridge before the process of igneous crustal accumulation was complete. A similar relationship between dipping intra-crustal reflections interpreted as faults and the Moho reflection was observed in the Blake Spur fracture zone area (White *et al.* 1990) and around the Canary Islands (Banda *et al.* 1992). White *et al.* (1990) suggested that, because the Moho is known to have formed away from the spreading ridge in some places in the North Atlantic (Bunch & Kennett 1980), we might expect intracrustal dipping structure that originally formed at the ridge to be truncated by a younger Moho reflector.

Fault-plane reflectivity

The fault-plane reflections are some of the brightest features observed in the igneous crust, comparable in amplitude to sea-floor and sediment reflections. Some of the lateral coherency may be due to smearing across the CMP gather since for a dipping reflector the true reflecting points are displaced up-dip relative to the midpoints (Levin 1971), although these reflections also appear bright on range-limited stacks (Fig. 15). The high reflectivity along faults cannot be explained merely by juxtaposition of adjacent blocks of differing impedance. Using near-normal incidence and wide-angle seismic data from the Early Cretaceous oceanic crust of the Blake Spur area, Minshull (1993) interprets dipping reflections in the upper crust to be zones of unusually high impedance produced by hydrothermal alteration in fault zones near the spreading centre. Mineralizing hydrothermal circulation along the upper part of the fault plane associated with newly emplaced igneous material at the spreading centre may contribute to the observed high reflectivity. Localized fault-controlled hydrothermal alteration, as deduced from ophiolite studies (Harper, Bowman & Kuhns 1988; Alexander *et al.* 1993), is an important process in the upper crust at the ridge. Furthermore, models relating normal-fault deformation, hydrothermal circulation, and magmatism imply that mineralization along faults is restricted to the upper igneous crust (i.e. where fluid pressure is hydrostatic) (Goldfarb & Delaney 1988; Sibson 1990; Alexander *et al.* 1993). Rona *et*

al. (1992) suggest that increased permeability along fault zones at the ridge may be responsible for locally enhanced circulation. Sea-bottom sampling studies at the modern Mid-Atlantic Ridge have detected strong hydrothermal discharge associated with serpentinized ultramafic rocks at fault intersections on the floor of the rift valley (Rona, Widenfalk & Boström 1987; Rona *et al.* 1992). The depth limit below the top of basement for this circulation is probably variable (Lister 1974; Christensen & Smewing 1981), but is thought to be 1–3 km (Mottl 1983) which may explain why the high reflectivity of the fault planes does not extend into the lowermost crust even though the fault planes can still be traced deeper as a lower amplitude reflection (e.g. 'W' Line 6).

Dipping reflections on strike lines

Because the strike (isochron) Lines 1 and 2, located along a magnetic-anomaly trend, span crust that is more or less the same age, we might expect a reflection pattern that represents a process that acted uniformly along the line. However, these profiles show little or no horizontal intracrustal features, but a bidirectional dipping fabric that includes reflections that are better developed, but less steep, than reflections on the flow profiles. The interpretation of the bidirectional fabric is not obvious. The lack of displacement of the top of basement or of any intracrustal horizons across these reflections suggests that they are not faults. The bidirectional sets differ significantly from the dipping reflections on the flow profiles by occurring in concordant packages rather than as single isolated reflections. Where line ties are possible, individual dipping isochron reflections correlate on the flow profiles to horizontal reflections. Fault-plane reflections on the flow profiles cannot be tied to reflections within the bidirectional sets.

In an attempt to explain non-horizontal fabrics, Mutter & Karson (1992) hypothesized that the various dipping reflectors within the igneous crust imaged on lines oriented in different directions can be explained as reflecting from a single low-angle normal-fault detachment with a complex 3-D structure; however, their interpretation was based on widely spaced seismic lines. The shallow-dipping reflections observed on the BIRPS strike profiles occur as two distinct directional sets and so cannot originate from a single surface. In some places, these reflections flatten into and merge with the Moho reflection. The close association of these reflections with the Moho reflection suggests that their formation is related to that of the Moho discontinuity itself, and thus implies a process of igneous construction. The correlation of the bidirectional sets with basement ridges further suggests an igneous origin. The fact that intracrustal reflections on the isochron profiles appear in bands, and not individually, supports a model of crustal growth by sill intrusion. Our observations are most consistent with a model in which oceanic crust forms from the successive intrusion of lens-shaped igneous sills (Sinton & Detrick 1992; Henstock, Woods & White 1993) rather than a single large magma chamber (Mutter *et al.* 1985; McCarthy *et al.* 1988).

CONCLUSIONS

(1) The essential factors in the design of the BIRPS survey included (a) deploying a large-capacity source rich in low frequencies for imaging deep structures in the crust with low s/n, but retaining sufficient high frequency to target detailed shallow sediment structure, (b) a low-noise shooting environment, and (c) a line spacing that is near to the lateral seismic resolution for the lower crust while wide enough to allow regional coverage.

(2) Owing to the great water depth, it was necessary to design a strategy to mitigate the effects of wrap-around multiples from the previous shot, as has contaminated other deep-water reflection surveys. To reduce the impact of these multiples and still record with a 50 m shot spacing, we adopted a random-shot time delay so that the multiples would tend to add destructively in the CMP domain.

(3) Isochron profiles display shallow-dipping packages of concordant reflections within the igneous crust occurring in bidirectional inclined sets. These sets appear to correlate with horizontal reflections on the flow profiles. We interpret these sets as magmatic, as opposed to tectonic, in origin and suggest that they are caused by successive intrusion of sills at the Early Cretaceous spreading ridge.

(4) Flow profiles show a completely different pattern involving steeper-dipping crustal reflections that occur singly and not in packages or bidirectional sets. The dominant dip direction is west towards the old spreading ridge. These reflections are usually planar and penetrate through all or most of the igneous crust. The close association of westward-dipping reflections with prominent offsets of the top of igneous basement indicates that these features are best interpreted as faults. Basement faults, which originally formed at the ridge crest, continue into normal-fault offsets in the sediments suggesting later reactivation or sediment consolidation. In some places, fault-plane reflections are enhanced in amplitude in the upper part of the igneous crust. The enhanced reflectivity observed may have been caused by mineralizing hydrothermal alteration in the upper part of the crust at the spreading ridge.

(5) Reflectivity of the Moho discontinuity, while well developed in some places, varies greatly across the small survey area. This variation is controlled in part by scattering from the top of igneous basement and thus is not always geologically significant. Moho reflections show a distinctly different structural relation to crustal features on the isochron and flow profiles: on isochron profiles, dipping reflections often flatten into, and may merge with, the Moho reflection; on flow profiles, as dipping crustal reflections approach the Moho, they are usually abruptly cut off by it without extending deeper. We interpret the faults to have developed initially at or near the spreading ridge before the process of igneous crustal accumulation was complete.

ACKNOWLEDGMENTS

BIRPS is supported by grants from the Natural Environment Research Council and our Industrial Associates (Amerada Hess Limited, Amoco Production Co., BP Exploration Co. Ltd, Chevron U.K. Ltd, Conoco (U.K.)

Ltd, Enterprise Oil PLC, Lasmo North Sea PLC, Mobil North Sea Ltd, and Shell U.K. Exploration and Production). We thank GECO-PRAKLA (particularly Marketing Manager Adrian Bligh) and Party Chief Rolf Henriksen for helping to make the cruise a success. R. W. England provided invaluable assistance as an observer at sea. Pre-stack processing was carried out by Simon Petroleum Technology Ltd in conjunction with BIRPS. Further data analysis for this study was performed on the GECO-PRAKLA Seismic Kernel System operating at Bullard Laboratories. Appreciation is expressed to S. Capon for assistance with the illustrations and to D. Simons for photography. T. A. Minshull provided useful criticism on an earlier version of the paper. Journal reviews by T. J. Reston and an anonymous referee also improved the paper. This is Department of Earth Sciences, University of Cambridge Contribution No. 3609.

REFERENCES

Alexander, R.J., Harper, G.D. & Bowman, J.R., 1993. Oceanic faulting and fault-controlled subseafloor hydrothermal alteration in the sheeted dike complex of the Josephine ophiolite, *J. geophys. Res.*, **98,** 9731–9759.

Allmendinger, R.W., Sharp, J.W., Von Tish, D., Serpa, L., Brown, L., Kaufman, S. & Oliver, J., 1983. Cenozoic and Mesozoic structure of the eastern Basin and Range province, Utah, from COCORP seismic-reflection data, *Geology*, **11,** 532–536.

Banda, E., Ranero, C.R., Dañobeitia, J.J. & Rivero, A., 1992. Seismic boundaries of the eastern Central Atlantic Mesozoic crust from multichannel seismic data, *Geol. Soc. Am. Bull.*, **104,** 1340–1349.

Beasley, C. & Mobley, E., 1988. Amplitude and anti-aliasing treatment in $(x-t)$ domain DMO, *Soc. Explor. Geophys., Expanded Abstracts.*

Bull, J.M. & Scrutton, R.A., 1992. Seismic reflection images of intraplate deformation, central Indian Ocean, and their tectonic significance, *J. geol. Soc. Lond.*, **149,** 955–966.

Bunch, A.W.H. & Kennett, B.L.N., 1980. The crustal structure of the Reykjanes Ridge at 59°30'N, *Geophys. J. R. astr. Soc.*, **61,** 141–166.

Carbotte, S. & Macdonald, K.C., 1990. Causes of variation in fault-facing direction on the ocean-floor, *Geology*, **18,** 749–752.

Chen, Y. & Morgan, W.J., 1990. A nonlinear rheology model for mid-ocean ridge axis topography, *J. geophys. Res.*, **95,** 17 583–17 604.

Christensen, N.I. & Smewing, J.D., 1981. Geology and seismic structure of the Oman ophiolite complex, *J. geophys. Res.*, **86,** 2245–2555.

Claerbout, J.F. 1985. *Imaging the Earth's Interior*, Blackwell Scientific Publications, Oxford.

Collins, J.A., Brocher, T.M., & Karson, J.A., 1986. Two-dimensional seismic reflection modeling of the inferred fossil oceanic crust/mantle transition in the Bay of Islands ophiolite, *J. geophys. Res.*, **91,** 12 520–12 538.

Cressman, K.S., 1968. How velocity layering and steep dip affect CDP, *Geophysics*, **33,** 399–411.

Dañobeitia, J.J. & Collette, B.J., 1989. Estudio mediante sismica de reflexión de un grupo de estructruras submarinas situadas al notre y sur del Archipielago Canario, *Acta Geol. Hispa.*, **24,** 147–163.

Dañobeitia, J.J. & Rivero, A. (reporters), 1991. *Estudio geofisico de la cuence oceánica al Oeste del Archipielago Canario*, Instituto Geográfico Nacional, Publicación Técnica núm. 25, Madrid, Spain.

Dauteuil, O. & Brun, J., 1993. Oblique rifting in a slow-spreading ridge, *Nature*, **361,** 145–148.

Dragoset, W., 1990. Airgun array specs: a tutorial, *Geophys. Lead. Edge Explor.*, **9,** 24–32.

Egan, M.S., Dingwall, K. & Kapoor, J., 1991. Shooting direction: A 3-D marine survey design issue, *Geophys. Lead. Edge Explor.*, **10,** 37–41.

Goldfarb, M.S. & Delaney, J.R., 1988. Response of two-phase fluids to fracture configurations within submarine hydrothermal systems, *J. geophys. Res.*, **93,** 4585–4594.

Harper, G.D., 1985. Tectonics of slow-spreading mid-ocean ridges and consequences of a variable depth to the brittle/ductile transition, *Tectonics*, **4,** 395–409.

Harper, G.D., Bowman, J.R. & Kuhns, R., 1988. Field, chemical, and isotopic aspects of submarine hydrothermal metamorphism of the Josephine ophiolite, Klamath mountains, California–Oregon, *J. geophys. Res.*, **93,** 4625–4657.

Hayes, D.E., Pimm, A.C., Beckmann, J.P., Benson, W.E., Berger, W.H., Roth, P.H., Supko, P.R. & von Rad, U., 1972. *Initial Reports of the Deep Sea Drilling Project, Volume XIV*, pp. 157–215, Washington (US Government Printing Office).

Hayes, D.E. & Rabinowitz, P.D., 1975. Mesozoic magnetic lineations and the magnetic quiet zone off northwest Africa, *Earth planet. Sci. Lett.*, **28,** 105–115.

Henstock, T.J., White, R.S. & McBride, J.H., 1994. Along axis variability in crustal accretion at the early Mesozoic Mid-Atlantic ridge: results from the OCEAN study, *J. geophys. Res.*, submitted.

Henstock, T.J., Woods, A.W. & White, R.S., 1993. The accretion of oceanic crust by episodic sill intrusion, *J. geophys. Res.*, **98,** 4143–4161.

Hobbs, R.W. & Snyder, D.B., 1992. Marine seismic sources used for deep seismic reflection profiling, *First Break*, **10,** 417–426.

Karson, J.A., 1990. Seafloor spreading on the Mid-Atlantic Ridge: Implications for the structure of ophiolites and oceanic lithosphere produced in slow-spreading environments, in *Ophiolites, oceanic crustal analogues*, pp. 547–555, eds Malpas, J.A. *et al.*, Geol. Surv. Dept., Nicosia, Cyprus.

Kent, D.V. & Gradstein, F.M., 1985. A Cretaceous and Jurassic geochronology, *Geol. Soc. Am. Bull.*, **96,** 1419–1427.

Klitgord, K.D. & Schouten, H., 1986. Plate kinematics of the Central Atlantic, in *The geology of North America, the western North Atlantic region*, Vol. M, pp. 351–377, eds Vogt, P.R. & Tucholke, B.E., Geol. Soc. Am., Boulder, CO.

Kong, L.S.L., Detrick, R.S., Fox, P.J., Mayer, L.A. & Ryan, W.B.F., 1988. The morphology and tectonics of the MARK area from Sea Beam and Sea MARC I observations (Mid-Atlantic Ridge 23°N), *Mar. geophys. Res.*, **10,** 59–90.

Larner, K., Chambers, R., Yang, M. & Wai, W., 1983. Coherent noise in marine seismic data, *Geophysics*, **48,** 854–886.

Levander, A., Smith, S.K., Hobbs, R.W., England, R.W., Snyder, D.B. & Holliger, K., 1994. The crust as a heterogeneous 'optical' medium or 'crocodiles in the mist', *Tectonophysics*, **232,** 281–297.

Levin, F.K., 1971. Apparent velocity from dipping interface reflections, *Geophysics*, **36,** 510–516.

Lister, C.R.B., 1974. On the penetration of water into hot rock, *Geophys., J. R. astr. Soc.*, **39,** 465–509.

Macdonald, K.C., Fox, P.J., Perram, L.J., Eisen, M.F., Haymon, R.M., Miller, S.P., Carbotte, S.M., Cormier, M.-H. & Shor, A.N., 1988. A new view of the mid-ocean ridge from the behaviour of ridge-axis discontinuities, *Nature*, **335,** 217–225.

Maschenkov, S. & Pogrebitsky, Y., 1992. Preliminary results of Canary–Bahamas Geotransect Project, *EOS, Trans., Am. geophys. Un.*, **73,** 393–397.

McBride, J.H., Lindsey, G.A., Hobbs, R.W., Snyder, D.B. & Totterdell, I.J., 1993. Some problems in velocity analysis for marine deep seismic profiles, *First Break*, **11,** 345–356.

McBride, J.H., Hobbs, R.W., Henstock, T.J. & White, R.S., 1994a. On the 'wraparound' multiple problem of recording seismic reflections in deep water, *Geophysics*, **59,** 1160–1165.

McBride, J.H., Henstock, T.J., White, R.S. & Hobbs, R.W., 1994b. Seismic reflection profiling in deep water: avoiding spurious reflectivity at lower-crustal and upper-mantle traveltimes, *Tectonophysics*, **232,** 425–435.

McCarthy, J., Mutter, J.C., Morton, J.L., Sleep, N.H. & Thompson, G.A., 1988. Relic magma chamber structures preserved within the Mesozoic North Atlantic crust?, *Geol. Soc. Am. Bull.*, **100,** 1423–1436.

Minshull, T.A., 1993. Wide-angle imaging of reflectors in Mesozoic oceanic crust, *Geophys. Res. Lett.*, **20,** 1619–1622.

Minshull, T.A., White, R.S., Mutter, J.C., Buhl, P., Detrick, R.S., Williams, C.A. & Morris, E., 1991. Crustal structure at the Blake Spur fracture zone from expanding spread profiles, *J. geophys. Res.*, **96,** 9955–9984.

Morris, E., Detrick, R.S., Minshull, T.A., Mutter, J.C., White, R.S., Su, W. & Buhl, P., 1993. Seismic structure of oceanic crust in the Western North Atlantic, *J. geophys. Res.*, **98,** 13 879–13 903.

Mottl, M.J., 1983. Metabasalts, axial hot springs, and the structure of hydrothermal systems at mid-ocean ridges, *Geol. Soc. Am. Bull.*, **94,** 161–180.

Mutter, J.C. & Karson, J.A., 1992. Structural processes at slow-spreading ridges, *Science*, **257,** 627–634.

Mutter, J.C. & North Atlantic Transect Study Group, 1985. Multichannel seismic images of the oceanic crust's internal structure: Evidence for a magma chamber beneath the Mesozoic Mid-Atlantic Ridge, *Geology*, **13,** 629–632.

NAT Study Group, 1985. North Atlantic transect: A wide-aperture, two-ship multichannel seismic investigation of the oceanic crust, *J. geophys. Res.*, **90,** 10 321–10 341.

Newman, P., 1984. Seismic response to sea-floor diffractors, *First Break*, **2,** 9–19.

Norrell, G.T. & Harper, G.D., 1988. Detachment faulting and amagmatic extension at mid-ocean ridges: The Josephine ophiolite as an example, *Geology*, **16,** 827–830.

Parkes, G.E. & Hatton, L., 1986. *The Marine Seismic Source*, Reidel, Dordrecht.

Peddy, C., Pinet, B., Masson, D., Scrutton, R., Sibuet, J.-C., Warner, M.R., Lefort, J.P. & Schroeder, I.J. (BIRPS & ECORS), 1989. Crustal structure of the Goban spur continental margin, northeastern Atlantic, from deep seismic reflection profiling, *J. Geol. Soc. Lond.*, **146,** 427–437.

Phipps Morgan, J. & Chen, Y.J., 1993. The genesis of oceanic crust: magma injection, hydrothermal circulation, and crustal flow, *J. geophys. Res.*, **98,** 6283–6297.

Raynaud, B.A., 1988. Statistical modelling of lower-crustal reflections, *Geophys. J. Int.*, **95,** 111–121.

Roberts, S., Andrews, J.R., Bull, J.M. & Sanderson, D.J., 1993. Slow-spreading ridge-axis tectonics: evidence from the Lizard complex, UK, *Earth planet. Sci. Lett.*, **116,** 101–112.

Roest, W.R., Dañobeitia, J.J., Verhoef, J. & Collette, B.J., 1992. Magnetic anomalies in the Canary Basin and the Mesozoic evolution of the central North Atlantic, *Mar. geophys. Res.*, **14,** 1–24.

Rona, P.A., Widenfalk, L. & Boström, K., 1987. Serpentinized ultramafic and hydrothermal activity at the Mid-Atlantic Ridge crest near 15°N, *J. geophys. Res.*, **92,** 1417–1427.

Rona, P.A., Bougault, H., Charlou, J.L., Appriou, P., Nelsen, T.A., Trefry, J.H., Eberhart, G.L., Barone, A. & Needham, H.D., 1992. Hydrothermal circulation, serpentinization, and degassing at a rift valley-fracture zone intersection: Mid-Atlantic Ridge near 15°N, 45°W, *Geology*, **20,** 783–786.

Rosendahl, B.R., Groschel-Becker, H., Meyers, J. & Kaczmarick, K., 1991. Deep seismic reflection study of a passive margin, southeastern Gulf of Guinea, *Geology*, **19,** 291–295.

Salisbury, M.H. & Keen, C.E., 1993. Listric faults imaged in oceanic crust, *Geology*, **21,** 117–120.

Scheirer, D.S. & Hobbs, R.W., 1990. Seismic attenuation in the continental crust SW of England, *Geophys. J. Int.*, **103,** 533–540.

Sempére, J.-C., Lin, J., Brown, H.S., Schouten, H. & Purdy, G.M., 1993. Segmentation and morphotectonic variations along a slow-spreading center: The Mid-Atlantic ridge (24°00'N–30°40'N), *Mar. geophys. Res.*, **15,** 153–200.

Sheriff, R.E., & Geldart, L.P., 1982. *Exploration Seismology Volume* 1, Cambridge University Press, Cambridge.

Sibson, R.H., 1990. Conditions for fault-valve behaviour, in *Deformation Mechanisms, Rheology and Tectonics*, eds Knipe, R.J. & Rutter, E.H., Geol. Soc. Spec. Publ., Lond., **54,** 15–28.

Sinton, J.M. & Detrick, R.S., 1992. Mid-ocean ridge magma chambers, *J. geophys. Res.*, **97,** 197–216.

Stolt, R.H. 1978. Migration by Fourier transform, *Geophysics*, **43,** 23–48.

Sundvik, M.T. & Larson, R.L., 1988. Sea floor spreading history of the western North Atlantic basin derived from the Keathley Sequence and computer graphics, *Tectonophysics*, **155,** 49–71.

Swift, S.A. & Stephen, R.A., 1989. Lateral heterogeneity in the seismic structure of upper oceanic crust, western North Atlantic, *J. geophys. Res.*, **94,** 9303–9322.

Sykes, L.R., 1978. Intraplate seismicity, reactivation of preexisting zones of weakness, alkaline magmatism, and other tectonism postdating continental fragmentation, *Rev. Geophys. Space Phys.*, **16,** 621–688.

Toomey, D.R., Soloman, S.C. & Purdy, G.M., 1988. Microearthquakes beneath the median valley of the Mid-Atlantic Ridge near 23°N: Tomography and tectonics, *J. geophys. Res.*, **93,** 9093–9112.

Tsai, C.J., 1985. A method to analyze and verify deep crustal reflections offshore Costa Rica, *Geophysics*, **50,** 196–206.

Turcotte, D.L. & Schubert, G., 1982. *Geodynamics Applications of Continuum Physics to Geological Problems*, John Wiley & Sons, New York.

Verhoef, J., Collette, B.J., Dañobeitia, J.J., Roeser, H.A. & Roest, W.R., 1991. Magnetic anomalies off West Africa (20°–38°N), *Mar. geophys. Res.*, **13,** 81–103.

White, R.S., 1984. Atlantic oceanic crust: Seismic structure of a slow-spreading ridge, in *Ophiolites and Oceanic Lithosphere*, eds Gass, I.G., Lippard, S.J. & Shelton, A.W. Geol. Soc. London Spec. Publ., **13,** 101–111.

White, N.J., Jackson, J.A. & McKenzie, D.P., 1986. The relationship between the geometry of normal faults and that of the sedimentary layers in their hanging walls, *J. struct. Geol.*, **8,** 897–909.

White, R.S., McBride, J.H., Henstock, T.J., & Hobbs, R.W., 1994. Internal structure of Mesozoic oceanic crust, *Geology*, **22,** 597–600.

White, R.S., Detrick, R.S., Mutter, J.C., Buhl, P., Minshull, T.A. & Morris, E., 1990. New seismic images of oceanic crustal structure, *Geology*, **18,** 462–465.

Whitmarsh, R.B., Miles, P.R. & Pinheiro, L.M., 1990. The seismic velocity structure of some NE Atlantic continental rise sediments; a lithification index?, *Geophys. J. Int.*, **101,** 367–378.

Wiens, D.A. & Stein, S., 1983. Age dependence of oceanic intraplate seismicity and implications for lithospheric evolution, *J. geophys. Res.*, **88,** 6455–6468.

Williams, C.A., Hill, I.A., Young, R. & White, R.S., 1990. Fracture zones across the Cape Verde Rise, NE Atlantic, *J. geol. Soc. Lond.*, **147,** 851–857.